This is a repository copy of *Mcidas mutant mice reveal a two-step process for the specification and differentiation of multiciliated cells in mammals*.

White Rose Research Online URL for this paper:
http://eprints.whiterose.ac.uk/143879/

Version: Published Version

Article:
Lu, H., Anujan, P., Zhou, F. et al. (4 more authors) (2019) Mcidas mutant mice reveal a two-step process for the specification and differentiation of multiciliated cells in mammals. Development, 146 (6). dev172643. ISSN 0950-1991

https://doi.org/10.1242/dev.172643

© 2019 Published by The Company of Biologists Ltd. Reproduced in accordance with the publisher's self-archiving policy.

Reuse
Items deposited in White Rose Research Online are protected by copyright, with all rights reserved unless indicated otherwise. They may be downloaded and/or printed for private study, or other acts as permitted by national copyright laws. The publisher or other rights holders may allow further reproduction and re-use of the full text version. This is indicated by the licence information on the White Rose Research Online record for the item.

Takedown
If you consider content in White Rose Research Online to be in breach of UK law, please notify us by emailing eprints@whiterose.ac.uk including the URL of the record and the reason for the withdrawal request.

eprints@whiterose.ac.uk
https://eprints.whiterose.ac.uk/

© 2019. Published by The Company of Biologists Ltd | Development (2019) 146, dev172643. doi:10.1242/dev.172643

RESEARCH ARTICLE

Mcidas mutant mice reveal a two-step process for the specification and differentiation of multiciliated cells in mammals

Hao Lu[1], Priyanka Anujan[1,2], Feng Zhou[1,*], Yiliu Zhang[1], Yan Ling Chong[1], Colin D. Bingle[2] and Sudipto Roy[1,3,4,‡]

ABSTRACT

Motile cilia on multiciliated cells (MCCs) function in fluid clearance over epithelia. Studies with *Xenopus* embryos and individuals with the congenital respiratory disorder reduced generation of multiple motile cilia (RGMC), have implicated the nuclear protein MCIDAS (MCI), in the transcriptional regulation of MCC specification and differentiation. Recently, a paralogous protein, geminin coiled-coil domain containing (GMNC), was also shown to be required for MCC formation. Surprisingly, in contrast to the presently held view, we find that *Mci* mutant mice can specify MCC precursors. However, these precursors cannot produce multiple basal bodies, and mature into single ciliated cells. We identify an essential role for MCI in inducing deuterosome pathway components for the production of multiple basal bodies. Moreover, GMNC and MCI associate differentially with the cell-cycle regulators E2F4 and E2F5, which enables them to activate distinct sets of target genes (ciliary transcription factor genes versus basal body amplification genes). Our data establish a previously unrecognized two-step model for MCC development: GMNC functions in the initial step for MCC precursor specification. GMNC induces *Mci* expression that drives the second step of basal body production for multiciliation.

KEY WORDS: Cilia, Multiciliated cell, GMNC, MCIDAS, E2F, Deuterosome

INTRODUCTION

The health of our airways is crucially dependent on mucociliary clearance, a process by which pathogen- and pollutant-laden mucus is cleared out by the beating of hundreds of motile cilia that decorate the surfaces of MCCs (Bustamante-Marin and Ostrowski, 2017). Ineffective mucus clearance predisposes individuals to respiratory diseases, best exemplified by congenital disorders such as primary ciliary dyskinesia (PCD) and RGMC (Knowles et al., 2016). In PCD, MCCs form normally, but their cilia are immotile or have defective motility owing to mutations in proteins required for the assembly or function of the motility apparatus. By contrast, in RGMC, differentiation of multiple cilia or the MCCs themselves is affected. MCCs are also present within brain ventricles, where they drive the circulation of cerebrospinal fluid, as well as within reproductive organs, where they promote mixing of reproductive fluids and germ cell transportation (Brooks and Wallingford, 2014; Zhou and Roy, 2015).

Post-mitotic MCC precursors support an explosive production of numerous basal bodies that migrate to the apical surface and nucleate the biogenesis of multiple motile cilia. One key aspect of MCC development is the transcriptional program required to institute its fate and its unique differentiation program, which has just begun to be elucidated (Spassky and Meunier, 2017). Studies with *Xenopus* embryos, which differentiate epidermal MCCs for mucus clearance, have implicated a small coiled-coil Geminin family protein, Mci (also known as multicilin), as a key regulator of MCC fate (Stubbs et al., 2012). Morpholino and shRNA-mediated inhibition of Mci function in the frog and cultured mouse brain MCC precursors resulted in a severe loss or significant reduction of MCC numbers, respectively, indicating an essential role for the protein in the specification and differentiation of these cells (Kyrousi et al., 2015; Stubbs et al., 2012). This phenotype has been shown to be largely conserved in individuals with RGMC carrying mutations in *MCIDAS*, which encodes human MCI, with their airways populated by cells differentiating only one or two immotile cilia (Boon et al., 2014). Conversely, overexpression of Mci in *Xenopus* embryos, as well as in cultures of airway and brain MCC precursors of the mouse is associated with the production of supernumerary MCCs (Kyrousi et al., 2015; Stubbs et al., 2012). Based on these findings, current view posits that, on the one hand MCI activity is essential for the transcription of genes encoding transcription factors (such as FOXJ1) that activate genes for ciliary differentiation and motility, and on the other genes for the production of multiple basal bodies (such as *Ccno*, *Deup1*, *Cep152* and *Ccdc78*) (Ma et al., 2014; Stubbs et al., 2012). MCI lacks a DNA-binding domain, and is thought to regulate transcription by associating with the cell-cycle transcriptional regulators E2F4 or E2F5, and their obligatory dimerization partner DP1 (Ma et al., 2014).

Recently, another MCI-related protein, GMNC (also known as GEMC1, Lynkeas), has been identified as an essential regulator of MCC development (Arbi et al., 2016; Kyrousi et al., 2015; Stubbs et al., 2012; Terré et al., 2016; Zhou et al., 2015). GMNC and MCI share significant homology (e.g. the human proteins share 47% identity overall), especially within a centrally located geminin coiled-coil domain and a C-terminal region, the so-called TIRT domain (named after the stretch of these four amino acids occurring twice within this domain in MCI proteins), which is thought to mediate interaction with the E2F factors (Ma et al., 2014; Terré et al., 2016). Zebrafish and mice with mutations in *Gmnc* are completely devoid of MCCs (Arbi et al., 2016; Terré et al., 2016; Zhou et al., 2015). At the molecular level, this includes a dramatic

[1]Institute of Molecular and Cell Biology, Proteos, 61 Biopolis Drive, Singapore 138673. [2]Academic Unit of Respiratory Medicine, Department of Infection, Immunity and Cardiovascular Disease, University of Sheffield, Sheffield S10 2JF, UK. [3]Department of Pediatrics, Yong Loo Lin School of Medicine, National University of Singapore, 1E Kent Ridge Road, Singapore 119288. [4]Department of Biological Sciences, National University of Singapore, 14 Science Drive 4, Singapore 117543.
*Present address: Global Academic Ventures, Suite 3, 531 Upper Cross Street, #03-11, Singapore 050531.

‡Author for correspondence (sudipto@imcb.a-star.edu.sg)

S.R., 0000-0002-6636-1429

Received 10 October 2018; Accepted 7 February 2019

Development (2019) 146, dev172643. doi:10.1242/dev.172643

loss of expression of genes such as *Foxj1* as well as genes required for the generation of multiple basal bodies, highly reminiscent of what has been described for MCI from *Xenopus* and human studies. Although there is some disagreement on the extent to which GMNC can interact with E2F4 versus E2F5 in transcriptional regulation (Terré et al., 2016; Zhou et al., 2015), nevertheless, like MCI, it can fully activate the transcriptional program for MCC specification and differentiation and produce supernumerary MCCs when overexpressed (Arbi et al., 2016; Kyrousi et al., 2015; Zhou et al., 2015). Endogenous expression of both *Mci* and *Gmnc* can be observed quite specifically in developing MCCs: GMNC acts upstream of MCI and is required for *Mci* expression in MCC precursors, whereas MCI is unable to induce *Gmnc* (Arbi et al., 2016; Kyrousi et al., 2015; Terré et al., 2016; Zhou et al., 2015). What remains presently unclear is how two related proteins, with purported similar transcriptional activities, can have near identical effects on the MCC developmental program.

Given this quandary, we re-investigated *Mci* function, this time by stably inactivating the gene in mice. We now show that, in contrast to the presently held belief that MCI regulates MCC specification as well as differentiation, *Mci* mutant mice can specify MCC precursors in normal numbers; these MCC precursors express a suite of genes for the transcriptional regulation of ciliary differentiation. However, these cells are unable to activate genes for basal body production, and consequently, differentiate single motile-like cilia. Moreover, we show that while MCI interacts with both E2F4 and E2F5, GMNC forms a complex more effectively with E2F5, with distinct C-terminal domains of the two proteins determining this differential interaction. We argue that MCC precursor specification and induction of transcription factors for ciliary gene expression is regulated by GMNC. In the next step, MCI amplifies the expression of ciliary transcription factors and triggers the expression of genes required for biogenesis of multiple basal bodies. These basal bodies then seed the assembly of multiple cilia to complete the process of MCC differentiation. Thus, our study provides mechanistic insight into how the regulatory activities of two paralogous proteins coordinately organize the transcriptional program of a highly specialized ciliated cell type.

RESULTS

Mci mutant mice cannot differentiate MCCs with multiple cilia

We used the CRISPR/Cas9 technology to generate a mutant allele of mouse *Mci*. This allele, a deletion of 32 bp in exon 2 of the *Mci* gene, is predicted to encode a severely C-terminally truncated MCI protein, lacking all of the important functional domains [the coiled-coil domain in the middle of the protein and the TIRT domain for E2F/DP1 interaction at the C-terminus (Ma et al., 2014)], implying a strong loss-of-function condition (see Materials and Methods; Fig. S1A-D). Heterozygous mice exhibited no phenotypic abnormalities, and, when intercrossed, homozygous wild type, heterozygous as well as homozygous mutants were recovered in the correct Mendelian ratio. However, the homozygous mutants were runts compared with their wild-type and heterozygous siblings, and showed progressive postnatal lethality (Fig. S2A-C). As *Gmnc* mutant mice also exhibit similar phenotypes, and their lethality has been attributed to the development of hydrocephalus (Terré et al., 2016), we examined *Mci* mutants for this defect. Indeed, histological analysis of the brains of two mutant animals (n=2) showed hydrocephalus, suggestive of dysfunctional ependymal MCCs (Fig. S2D,E). Moreover, all homozygous mutants tested (males and females) failed to breed, when in-crossed as well as when out-crossed, indicating MCC defects in the reproductive organs. To adduce evidence that the production of the wild-type MCI protein is indeed disrupted in the homozygotes, we cloned the mutant *Mci* cDNA from tracheal tissue and confirmed the presence of the 32 bp deletion (Fig. S1E). In addition, quantitation of *Mci* transcript levels from cultures of airway cells from the homozygotes revealed severe reduction relative to wild type (see Fig. 4).

We next investigated the status of MCCs in tissues where they are normally known to differentiate – trachea, oviducts and brain ependyma (Brooks and Wallingford, 2014; Spassky and Meunier, 2017; Zhou and Roy, 2015). In the wild type, abundant MCCs with multiple motile cilia were visible decorating the lumenal surface of these tissues, interspersed with other cell types (Fig. 1A,B and Fig. S2F,G). By contrast, in the mutants we found a complete loss of the multiple ciliated cells (Fig. 1C,D and Fig. S2F,G). Instead, we could observe cells with a single cilium. The length and width of these monocilia were similar to the multiple cilia of MCCs, but distinctly different from the shorter, thinner primary cilia present on neighboring cells (Fig. 1C). Even though the *Mci* mutants develop hydrocephalus and are infertile, because these mice are maintained under specific-pathogen-free (SPF) conditions, we did not detect any obvious symptoms of airway disease either at the behavioral level or through histopathological analysis of respiratory tissues (data not shown).

In *Mci* mutants, MCC precursors are specified but fail to generate multiple basal bodies

To begin to uncover the developmental defect underlying MCC absence in *Mci* mutants, we first analyzed the expression of FOXJ1, a protein that is required to activate the motile cilia-specific transcriptional program (Choksi et al., 2014a; Stubbs et al., 2008;

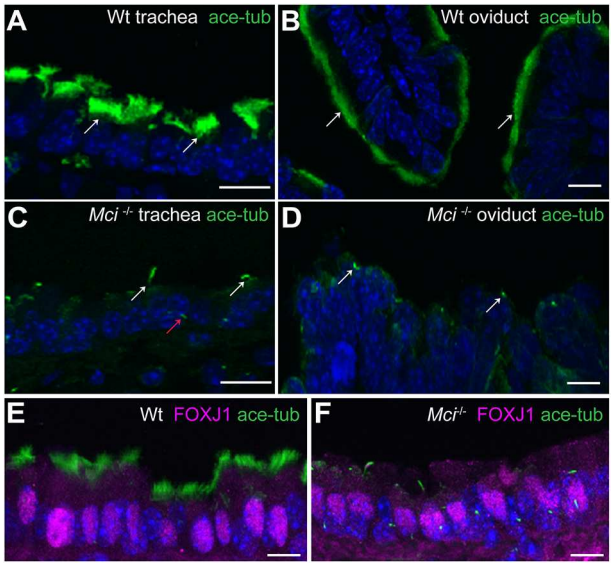

Fig. 1. MCCs in *Mci* mutant mice differentiate a single cilium and express FOXJ1. (A) Wild-type trachea section showing multiple cilia on MCCs (arrows). (B) Wild-type oviduct section showing multiple cilia on MCCs (arrows). (C) *Mci* mutant trachea section showing cells with a single cilium (white arrows). A primary cilium in a neighboring cell is indicated (red arrow). (D) *Mci* mutant oviduct section showing cells with a single cilium (arrows). (E) Nuclear-localized FOXJ1 expression in MCCs of wild-type trachea. (F) Nuclear-localized FOXJ1 expression in monociliated cells of *Mci* mutant trachea. In all preparations, cilia were stained using anti-acetylated tubulin antibodies (green) and nuclei with DAPI (blue). Wt, wild type. Scale bars: 10 µm. For all histological data in this and subsequent figures, tissues from at least two wild-type and three *Mci* mutant mice were analyzed unless mentioned otherwise.

Development (2019) 146, dev172643. doi:10.1242/dev.172643

Yu et al., 2008). Previous studies with *Xenopus* embryos and human airway cells have shown that *Foxj1* expression is strongly reduced in the absence of Mci activity (Boon et al., 2014; Stubbs et al., 2012). Strikingly, and contrary to these earlier findings, FOXJ1 expression was not affected in MCC harboring tissues of *Mci* mutant mice. Although FOXJ1 was present in the nucleus of wild-type MCCs, in the mutants, we found nuclear-localized FOXJ1 in cells bearing single long cilium (Fig. 1E,F and Fig. S2F,G). Based on this observation, we reasoned that the absence of MCI function perhaps does not compromise the specification of MCC precursors, but instead is required in these cells to differentiate multiple cilia. To bolster this view, we analyzed the expression of a suite of additional transcription factors that, like FOXJ1, have been implicated in motile ciliogenesis: RFX2, RFX3 and TAP73 (Choksi et al., 2014b; Jackson and Attardi, 2016). Again, like FOXJ1, expression of these transcription factors was not discernably affected (Fig. 2A-F). These findings suggest that, in the absence of MCI function, MCC precursors are specified normally, but they then differentiate a single cilium instead of multiple cilia. To garner evidence that this single cilium possesses attributes of motile cilia, we stained tracheal sections with antibodies against three unique structural constituents of the motile cilia, RSPH1 and RSPH9 [two radial spoke-head proteins (Frommer et al., 2015)], as well as CCDC40 [an axonemal component (Becker-Heck et al., 2011)]. The single cilium of *Mci* mutants showed localization of all three proteins along the axoneme (Fig. 2G-J and Fig. S3A-H). We also examined the status of the MCCs in the trachea using scanning electron microscopy (SEM). Unlike in the wild type, where hundreds of motile cilia were present at the apical surface of the MCCs, *Mci* mutant trachea showed cells with a single cilium whose dimensions were similar to an individual motile cilium of wild-type MCCs (Fig. 2K,L).

Since MCC differentiation is contingent upon the generation of multiple basal bodies, we next investigated the status of these organelles. Staining with anti-pericentrin antibodies revealed multiple basal bodies in wild-type MCCs, neatly arrayed along their apical membranes (Fig. 3A). By contrast, in *Mci* mutants, we could observe a single basal body associated with the single cilium (Fig. 3B). We obtained similar data with antibodies to γ-tubulin, which also labels ciliary basal bodies (data not shown; but see next section). Thus, the program for multiple basal body generation is significantly derailed in *Mci* mutants. We used transmission electron microscopy (TEM) to analyze the basal body phenotype in greater subcellular detail. Although cilia-bearing multiple basal bodies were readily visible in wild-type MCCs, in the mutants they were absent from several sections that we examined (Fig. 3C,D).

In vitro culture of *Mci* mutant airway cells revealed a strong impairment in expression of basal body generation genes

To uncover the earliest developmental defects in *Mci* mutant MCCs, we resorted to culturing mouse tracheal epithelial cells (mTECs) *in vitro*, followed by differentiation under air-liquid interface (ALI) conditions. Consistent with our observations from trachea, brain and oviduct sections, mTECs from *Mci* mutant mice differentiated single cilium-bearing cells, unlike the wild-type, where MCCs readily formed (Fig. 3E,F). Moreover, expression of FOXJ1 was not affected in *Mci* mutant cultures (Fig. 3G,H), implying that, as *in vivo*, loss of MCI does not compromise the ability to adopt the MCC precursor identity (RSPH proteins also localized to the single

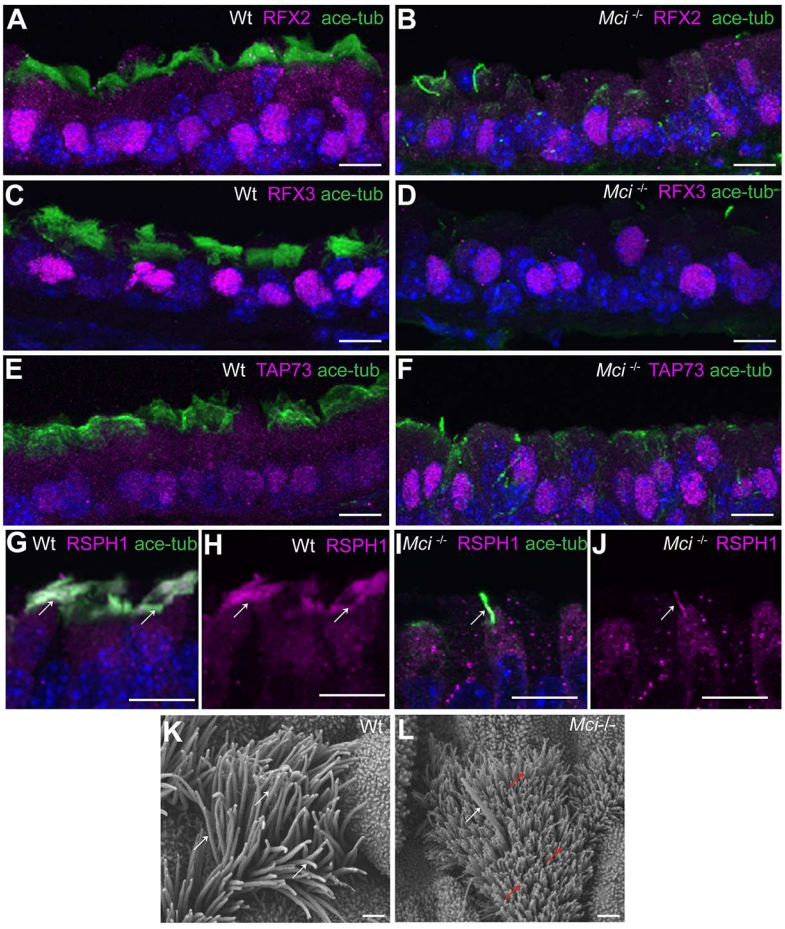

Fig. 2. *Mci* mutant MCC precursors express a suite of ciliary transcription factors and their single cilium localizes motile cilia-specific proteins. (A) Nuclear-localized RFX2 expression in MCCs of wild-type trachea. (B) Nuclear-localized RFX2 expression in monociliated cells of *Mci* mutant trachea. (C) Nuclear-localized RFX3 expression in MCCs of wild-type trachea. (D) Nuclear-localized RFX3 expression in monociliated cells of *Mci* mutant trachea. (E) Nuclear-localized TAP73 expression in MCCs of wild-type trachea. (F) Nuclear-localized TAP73 expression in monociliated cells of *Mci* mutant trachea. (G) RSPH1 colocalization with acetylated tubulin to MCC cilia of wild-type trachea (arrows). (H) RSPH1 localization to MCC cilia of wild-type trachea (arrows; display of only RPSH1 staining from G). (I) RSPH1 colocalization with acetylated tubulin to a single cilium of *Mci* mutant trachea (arrow). (J) RSPH1 localization to single cilium of *Mci* mutant trachea (arrow; display of only RSPH1 staining from I). (K) SEM analysis of a wild-type tracheal MCC showing multiple cilia (arrows). (L) SEM analysis of *Mci* mutant MCCs with a single cilium (white arrow). The microvilli, which are longer in the MCCs and normally remain obscured by the multiple cilia, are indicated (red arrows). One wild-type and one mutant trachea were scanned by SEM. The single-cilium phenotype of the *Mci* mutant trachea is representative of several fields of view scanned by SEM. In all preparations, cilia were stained using anti-acetylated tubulin antibodies (green) and nuclei with DAPI (blue). Scale bars: 10 µm in A-J; 5 µm in K,L.

Development (2019) 146, dev172643. doi:10.1242/dev.172643

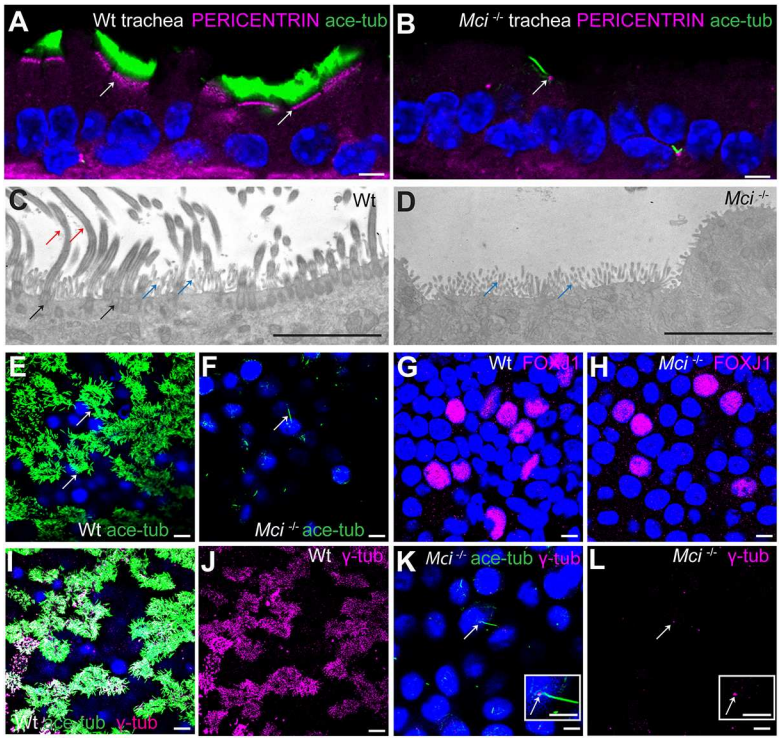

Fig. 3. *Mci* mutant MCC precursors are unable to generate multiple basal bodies. (A) A wild-type trachea section showing apically aligned multiple basal bodies in MCCs (arrows; stained using anti-pericentrin antibodies). (B) Section of *Mci* mutant trachea showing single basal body in monociliated cells (arrows). (C) TEM image showing multiple basal bodies (black arrows) and cilia (red arrows) in a wild-type MCC. Microvilli are also indicated (blue arrows). (D) TEM image showing lack of multiple basal bodies and cilia in a *Mci* mutant MCC. Microvilli are indicated (blue arrows). Five sections each from two independent wild-type and mutant tracheae were sampled, and the cells were examined from the basal to the apical end. We did not find any evidence of undocked basal bodies in the cytoplasm of *Mci* mutant cells. (E) Wild-type MCCs differentiated in ALI culture with multiple cilia (arrows). (F) *Mci* mutant airway cells differentiated in ALI culture with a single cilium (arrow). (G) Wild-type airway cells differentiated in ALI culture showing nuclear FOXJ1 expression. (H) *Mci* mutant airway cells differentiated in ALI culture showing nuclear FOXJ1 expression. (I) Wild-type MCCs differentiated in ALI culture with multiple basal bodies (stained with anti-γ-tubulin antibodies) and multiple cilia. (J) Display of only γ-tubulin staining from I. (K) *Mci* mutant cells differentiated in ALI culture with a single basal body (arrow) and a single cilium. Inset shows a single cilium and basal body (arrow). (L) Display of only γ-tubulin staining from K showing a single basal body (arrow). Inset shows a single basal body (arrow). In preparations shown in A,B,E,F,I,K, cilia were stained using anti-acetylated tubulin antibodies (green) and nuclei were stained with DAPI (blue). Scale bars: 5 µm. ALI cultures were carried out in three independent biological replicates.

cilium of ALI cultured cells (data not shown). Moreover, γ-tubulin staining revealed absence of multiple basal bodies, whereas wild-type MCCs showed clouds of basal bodies at their apical surface (Fig. 3I-L). We obtained a similar result with antibodies against the centrin protein that also marks the basal bodies (Fig. S3I-L). Thus, *in vivo* as well as *ex vivo*, loss of MCI specifically compromises the ability of MCC precursors to generate multiple basal bodies.

We next used RT-qPCR analysis to interrogate the transcriptional profile of the *Mci* mutant cells through the differentiation process. Whereas levels of *Mci* transcripts were strongly reduced, expression of genes encoding upstream transcription regulatory factors, such as GMNC, FOXJ1 and the RFX family members RFX2 and RFX3, were not appreciably affected or were slightly reduced relative to wild type (Fig. 4A-E). This lack of a major reduction is consistent with our observations using immunofluorescence analysis, described above. By contrast, genes implicated in the production of multiple basal bodies – *Deup1*, *Ccdc78*, *Ccno* and *Cdc20b* – were all strongly reduced, indicating that MCI is specifically required to activate their transcription (Fig. 4F-I).

In *Mci* mutant MCC precursors, deuterosomes are severely reduced in number and are dysfunctional

The current view posits two distinct pathways for multiple basal body generation in MCCs. Some of the basal bodies are believed to be generated by the mother centriole-dependent (MCD) pathway, through the activity of proteins such as CEP63, CEP152, PLK4 and SAS6, which also function in centriole duplication during regular cell division (Al Jord et al., 2014; Spassky and Meunier, 2017). In addition to this, a dedicated pathway exists in the MCCs for basal body generation. The vast majority of basal bodies are produced by this alternative mechanism – the deuterosome-dependent (DD) pathway – in which DEUP1, CCNO, CCDC78 and CDC20B are believed to be dedicated components (Funk et al., 2015; Klos Dehring et al., 2013; Revinski et al., 2018; Spassky and Meunier, 2017; Zhao et al., 2013). Here, electron-dense structures called deuterosomes are first generated by the oligomerization of the CEP63 paralog DEUP1. Although whether the deuterosomes are nucleated by existing centrioles or arise *de novo* is presently a matter of considerable debate (Al Jord et al., 2014; Mercey et al., 2018preprint; Nanjundappa et al., 2018preprint; Zhao et al., 2018preprint), what is clear is that, after formation, they recruit CEP152 and other MCD pathway proteins (PLK4, SAS6, etc.) to generate multiple procentrioles. These procentrioles then mature into centrioles, detach and migrate apically to dock with the plasma membrane and form ciliary basal bodies.

We found that, despite the strong reduction in *Deup1* mRNA levels in the *Mci* mutants, DEUP1-positive deuterosomes nevertheless formed, albeit in significantly reduced numbers

Development (2019) 146, dev172643. doi:10.1242/dev.172643

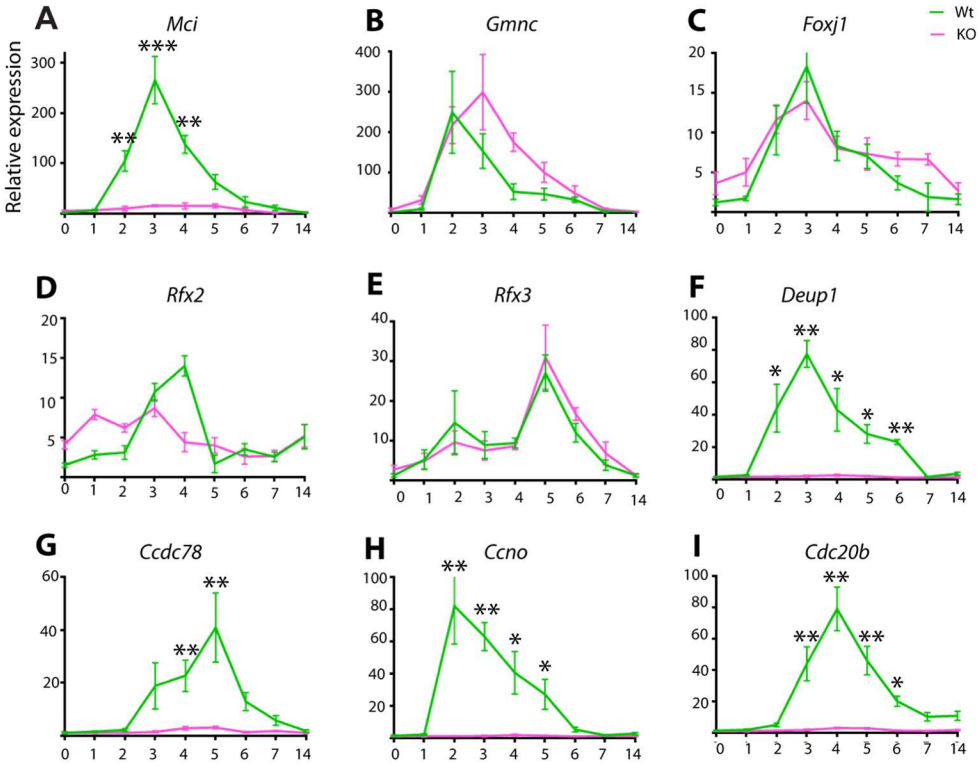

Fig. 4. RT-qPCR analysis of ciliary transcription factor and DD pathway gene expression levels between wild-type and *Mci* mutant airway cells in ALI culture. (A-I) Relative expression levels are plotted on the *y*-axis, and days in ALI culture are plotted on the *x*-axis. KO, *Mci* mutant. Data are mean±s.e.m. Analysis was carried out on three independent biological replicates. **P*<0.05; ***P*<0.01; ****P*<0.001.

(Fig. 5A-E). However, as we consistently failed to detect multiple centrioles in *Mci* mutant MCCs *ex vivo* as well as *in vivo*, these must be defective deuterosomes incapable of supporting centriole biogenesis. The complete absence of centriole duplication in *Mci* mutants suggests that even the MCD pathway is defective. To investigate this issue further, we examined expression of the MCD pathway gene *Cep63*, as well as *Cep152*, *Plk4* and *Sas6* (which are shared by both DD and MCD pathways), but failed to detect any major difference in their expression levels (Fig. 5F-I).

GMNC and MCI have distinct effects on the MCC-specific transcriptional program

In *Gmnc* mutant mice, the expression of the entire MCC-specific transcriptional program is significantly dampened (Terré et al., 2016). This includes: (1) genes for ciliary transcription factors such as FOXJ1 and MCI, as well as (2) genes for DD (but not MCD) pathway proteins. On the other hand, our current analysis shows that MCI loss preferentially affects the DD pathway genes. To examine this differential effect, we first overexpressed the human homologs of GMNC and MCI individually in HEK293T cells, and monitored the expression of genes from the two sets mentioned above. Terré et al. have previously demonstrated that HEK293T cells can be used effectively to assess the transcriptional activities of GMNC and MCI (Terré et al., 2016). GMNC could induce *MCI*; however, overexpression of MCI could not induce *GMNC* (Fig. 6A,B), which is consistent with previous reports (Arbi et al., 2016; Terré et al., 2016). Interestingly, both GMNC and MCI were able to induce *FOXJ1* (Fig. 6C). With respect to DD pathway genes, MCI alone or MCI together with GMNC strongly upregulated *DEUP1*, *CCNO* and *CDC20B* (Fig. 6D-F), although there was no significant additive effect from the co-expression. However, GMNC alone could only weakly induce these genes (Fig. 6D-F). These data support the idea that MCI preferentially affects the expression of DD pathway genes (also see below).

As MCI, and also GMNC, have been reported to interact with E2F4 and E2F5 for transcription, we next checked the transcriptional abilities of GMNC and MCI when co-expressed with E2F4 or E2F5. The ability of GMNC to induce *MCI* and *FOXJ1* was strongly increased with E2F5, but not with E2F4 (Fig. 6G,H). Likewise, a slight upregulation of DD pathway genes occurred when GMNC was overexpressed with E2F5, but not with E2F4 (Fig. 6I-K). By contrast, MCI with E2F4 or E2F5 had stronger transcriptional effect on *DEUP1*, *CCNO* and *CDC20B* than MCI alone (Fig. 6I-K). With regard to *FOXJ1*, MCI with E2F4 as well as E2F5 could induce higher levels of transcription than MCI alone, and MCI with E2F4 was more efficient than MCI with E2F5 (Fig. 6H). Thus, the transcriptional activity of GMNC appears to be much more effective with E2F5, whereas MCI can regulate its target genes with either E2F4 or E2f5.

Differential interaction of E2F4 and E2F5 with MCI and GMNC

We have previously shown that human GMNC is unable to interact effectively with E2F4 (Zhou et al., 2015). However, using a similar assay, Terré et al. demonstrated that GMNC can interact with E2F4 as well as E2F5 (Terré et al., 2016). Moreover, E2F5 has been shown to significantly potentiate the transcriptional activity of GMNC (Arbi et al., 2016). As our current analysis shows that GMNC and MCI act in a step-wise manner and regulate distinct sets of targets, we re-evaluated their interactions with the E2F factors. Consistent with our earlier report, human as well as mouse GMNC interacted poorly with human and mouse E2F4 and DP1, respectively (Fig. 7A,B). By contrast, we found robust interaction of human and mouse GMNC with human and mouse E2F5 and DP1, respectively (Fig. 7A,B). As a control, we found that as reported before (Ma et al., 2014), MCI proteins from both species interacted equally efficiently with E2F4 and E2F5 (Fig. 7A and Fig. S4A).

The E2F/DP1 interaction domain in MCI is located at the C-terminal end (~40 amino acids – the TIRT domain) (Ma et al., 2014;

Development (2019) 146, dev172643. doi:10.1242/dev.172643

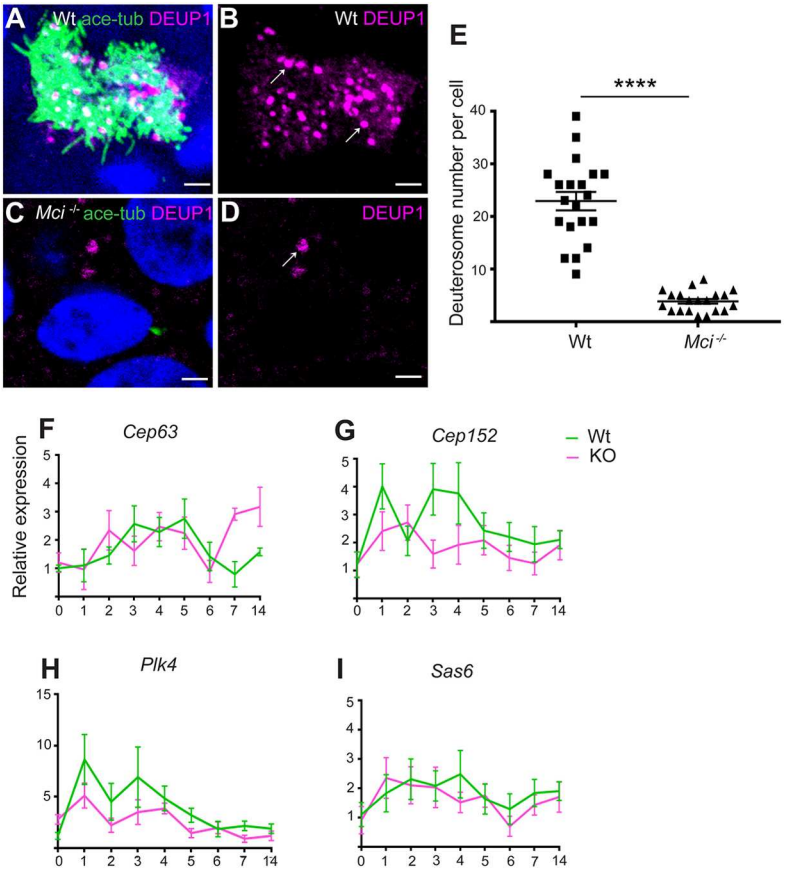

Fig. 5. In *Mci* mutants, the DD pathway for basal body production is strongly affected but not the MCD pathway. (A) ALI cultured wild-type MCCs showing DEUP1-positive deuterosomes. (B) Display of only DEUP1 staining from A, showing deuterosomes (arrows). (C) ALI-cultured *Mci* mutant airway cells showing DEUP1-positive deuterosomes. (D) Display of only DEUP1 staining from C, showing a deuterosome (arrow). Scale bars: 5 µm. (E) Quantification of the numbers of DEUP1^{+} deuterosomes in differentiating wild-type and *Mci* mutant MCCs under ALI conditions. Twenty cells were counted for each genotype at ALI day 3. ****$P \leq 0.0001$. (F-I) RT-qPCR analysis of MCD pathway gene expression levels between wild-type and *Mci* mutant airway cells in ALI culture. Relative expression levels are plotted on the *y*-axis, and days in ALI culture on the *x*-axis. Data are mean±s.e.m. Analysis was carried out on three independent biological replicates.

Stubbs et al., 2012). Even though GMNC shares significant homology with MCI in this region (Terré et al., 2016), the TIRT residues are not well conserved in the former, implying some divergence in the functionality of this domain between the two proteins (Fig. S4B). We replaced this domain in GMNC with the one from MCI (Fig. S4B), and then examined the interaction of the chimera (GM) with E2F4 and E2F5. Similar to MCI, but unlike wild-type GMNC, the GM chimera efficiently bound E2F4 as well as E2F5 (Fig. 7B). Despite this, GM overexpression alone or in combination with the E2F factors failed to elicit a transcriptional response in HEK293T cells, indicating that association with E2F4 by itself is not sufficient to switch the transcriptional activity pattern of GMNC towards that of MCI (Fig. S4C,D).

MCI can substitute for GMNC, but GMNC cannot substitute for MCI, in MCC formation

Last, we investigated whether GMNC and MCI can substitute for each other in MCC development. As the function of GMNC in MCC formation is highly conserved between zebrafish and mice (Arbi et al., 2016; Terré et al., 2016; Zhou et al., 2015), we first overexpressed mouse MCI in *gmnc* mutant zebrafish embryos, which completely lack MCCs from all MCC-bearing tissues, and found very efficient rescue of MCCs within the pronephric (kidney) ducts, where these cells function to promote urine flow (Fig. 8A-C). For the converse experiment, we used lentivirus-mediated human GMNC overexpression in mTEC ALI cultures from *Mci* mutant and wild-type mice. Although GMNC produced ectopic MCCs in the wild type, it failed to rescue MCC development in *Mci* mutant cultures (Fig. 8D-G and Fig. S5A,B,D). Moreover, although GMNC overexpression in *Mci* mutant cells could induce *Mci*, *Foxj1* and *Rfx3*, DD pathway genes were not upregulated (Fig. S6A, B,D-F and data not shown). This observation suggests that the weak induction of DD pathway genes on overexpression of GMNC in HEK293T cells that we noted earlier (cf. Fig. 6D-F), could possibly occur via GMNC-dependent induction of MCI. By contrast, human MCI overexpression generated significant numbers of MCCs in wild-type as well as *Mci* mutant cultures, denoting effective rescue, and also induced high levels of *Foxj1* and DD pathway genes (Fig. 8H,I and Figs S5A,C,D and S6C-F). Both the human *GMNC* and *MCI* genes were clearly overexpressed in these experiments (Fig. S5E,F), so the inability of GMNC to rescue is unlikely to be due to inadequate levels. Moreover, expression of *E2f4*, *E2f5* and *Dp1* was also not affected in *Mci* mutant cells (data not shown), and therefore, cannot also account for the lack of rescue of MCC formation by GMNC.

DISCUSSION

Using *Mci* mutant mice, we have established two distinct steps in the developmental pathway for MCC formation that had remained previously unrecognized and are genetically separable: first, GMNC acts to specify MCC precursors, whereas in the second step, MCI drives multiple basal body production and multiciliation. Thus, in the absence of GMNC function, the MCC-specific developmental program is blocked at the earliest step, and no MCC precursors are generated (Arbi et al., 2016; Terré et al., 2016; Zhou et al., 2015). By contrast, loss of MCI does not derail MCC precursor specification, but affects their subsequent differentiation into MCCs. MCI amplifies the expression of the ciliary transcription factor genes that are initially activated by GMNC, and induces the DD-pathway genes for basal body generation. Thus, even though there is an overlap in the regulation of genes encoding ciliary transcription factors by GMNC and MCI, our data suggest that the

Development (2019) 146, dev172643. doi:10.1242/dev.172643

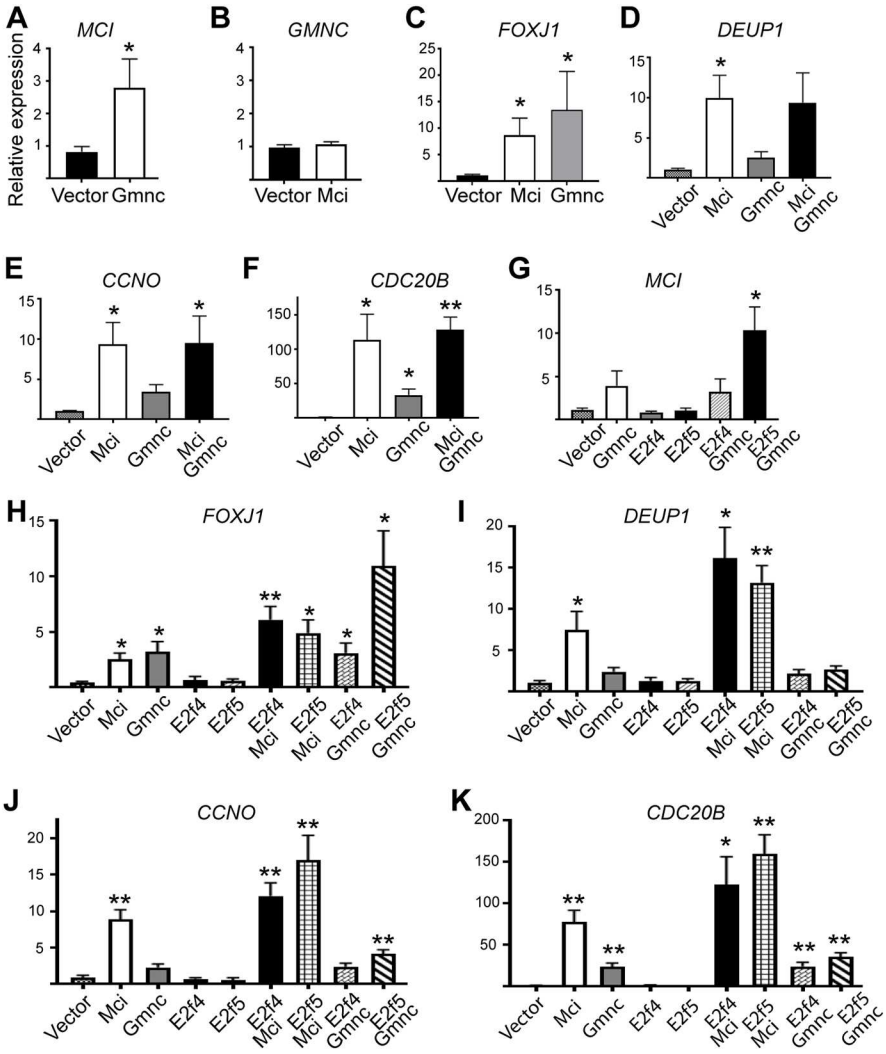

Fig. 6. RT-qPCR analysis of ciliary transcription factor and DD pathway gene expression levels in response to overexpression of MCI, GMNC and E2F proteins in HEK293T cells. (A-K) Relative expression levels are plotted on the *y*-axis; overexpression conditions are indicated on the *x*-axis. Data are mean±s.e.m. Analysis was carried out on three independent biological replicates. *$P \leq 0.05$, **$P \leq 0.01$.

DD-pathway genes are targeted exclusively by MCI. We have, however, noted that, despite the strong reduction in mRNA levels of an important DD pathway gene, *Deup1*, in *Mci* mutant cells, some Deup1 protein is synthesized and assembles into a few deuterosomes. Although this observation implies that *Deup1* transcription can occur to some extent even in the absence of MCI function and that this could be mediated by GMNC, at the moment we are unable to discount the contribution of several other ciliary transcription factors such as FOXJ1 and the RFX proteins (which are abundantly expressed in the *Mci* mutant MCC precursors) or a completely different transcriptional pathway for this expression of *Deup1* (and perhaps other DD pathway genes) in *Mci* mutant cells (also see below a discussion on GMNC-MCI-independent regulation of MCD pathway genes in developing MCCs). In fact, the inability of GMNC to induce the DD pathway genes when overexpressed at high levels in *Mci* mutant cells adds credence to this possibility. Alternatively, GMNC activity could be permissive, but not sufficient, for the induction of the DD pathway genes. In any case, our data clearly make a distinction between the transcriptional abilities of GMNC and MCI that had not been appreciated before, and show how regulation of the MCC developmental program is partitioned between the two paralogues. Although the discrepancy between our findings and the currently held notion of MCI activity (required for MCC specification and differentiation) could stem from species-specific differences in the requirement of the protein in MCC formation, it is possible that differences in strategies used to interrogate MCI in mice and frogs (genetic mutation in mice versus morpholino knock-down in frogs), as well as methods used to examine MCC status on MCI loss in mice and humans (*in vivo* and *ex vivo* analysis of MCCs from multiple mouse ciliated tissues versus MCCs obtained from individuals with RGMC using nasal brush biopsy) (Boon et al., 2014; Stubbs et al., 2012) are also responsible.

Although MCC precursors form in the *Mci* mutants and express several transcription factors necessary for ciliary differentiation and motility, they consistently differentiate into cells with a single motile-like cilium. We found no evidence for multiple basal bodies using several markers of these organelles and TEM analysis. As some MCC basal bodies are thought to be produced via the MCD pathway (Al Jord et al., 2014), our observation that there is consistently only one basal body in *Mci* mutant MCCs suggests that, along with the DD pathway, the MCD pathway is also strongly impaired. Yet we did not detect major changes in the levels of several important MCD pathway genes, the expression of which, like the DD pathway genes, is elevated during MCC differentiation (our data and Terré et al., 2016; Zhao et al., 2013). Such a lack of effect on the MCD pathway genes has also been reported previously for the *Gmnc* mutant mice (Terré et al., 2016), indicating that these genes are regulated independently of the GMNC-MCI network. Moreover, as recent reports show that MCC precursors devoid of

Development (2019) 146, dev172643. doi:10.1242/dev.172643

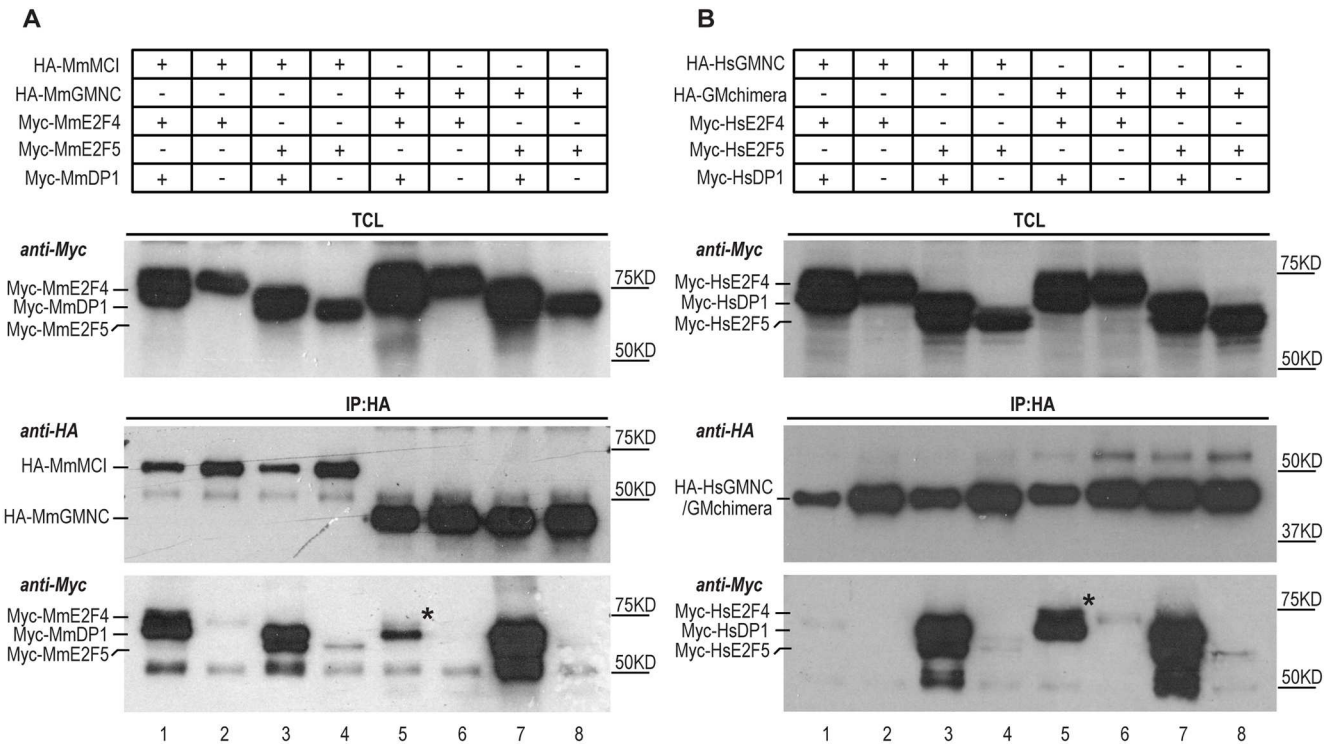

Fig. 7. Differential interaction of MCI and GMNC with E2F4 and E2F5. (A) Co-immunoprecipitation experiments using mouse (Mm, *Mus musculus*) proteins show that MCI effectively interacted with both E2F4 and E2F5 in the presence of DP1 (lane 1, IP panel, anti-Myc blot); very little E2F4 co-precipitated with GMNC and DP1 (lane 5, IP panel, anti-Myc blot). The weak presence of E2F4 in the GMNC IP is marked by the black asterisk. (B) The C-terminal domain of MCI accounts for effective interaction with both E2F4 and E2F5. GMNC showed minimal interaction with E2F4 (lane 1, IP panel, anti-Myc blot). In comparison, the GM (engineered by replacing the C-terminal domain of GMNC with that of MCI) chimera could co-precipitate with both E2F4 and E2F5, in the presence of DP1 (lane 5 and 7, IP panel, anti-Myc blot). The black asterisk marks the E2F4 band that is absent in lane 1 (IP panel, anti-Myc blot). Human (Hs, *Homo sapiens*) proteins were used for this experiment. The E2F and DP1 proteins were tagged N terminally with the Myc epitope, and the GMNC and MCI proteins were tagged N terminally with the HA epitope. TCL, total cell lysate; IP, immunoprecipitation. Data are representative of two independent biological replicates.

both mother and daughter centrioles can fully generate deuterosomes and multiple basal bodies (Mercey et al., 2018preprint; Nanjundappa et al., 2018preprint; Zhao et al., 2018preprint), these findings and our current data can be taken to indicate that the MCD pathway may not function in MCCs at all, at least in the tracheal MCCs, which we have investigated in sufficient detail, and all of the basal bodies in these cells could arise exclusively via the DD pathway. Given all of the present ambiguity by which the deuterosomes and basal bodies arise in the MCCs (Al Jord et al., 2014; Mercey et al., 2018preprint; Nanjundappa et al., 2018preprint; Zhao et al., 2018preprint), the *Mci* mutant mice are indeed a valuable reagent for deciphering the precise mechanisms involved in these intriguing processes.

Finally, we have provided some biochemical evidence for the difference in the transcriptional activities of GMNC and MCI, which could explain the distinct MCC phenotypes observed when they are individually mutated. In a side-by-side comparison with mouse as well as human homologs, we found that GMNC interacts much more efficiently with E2F5 than with E2F4, whereas MCI interacts equally well with both E2F4 and E2F5. In addition, replacement of the C-terminal region of GMNC with that from MCI, conferred on the chimeric protein the ability to interact with E2F4. Furthermore, our data show that GMNC is more effective in inducing *FOXJ1* and *MCI*, whereas MCI is more effective in inducing genes involved in basal body generation. When they are overexpressed with E2F4 or E2F5, GMNC is able to induce its targets much more efficiently with E2F5, whereas MCI largely fares equally well with E2F4 and E2F5. These data suggest that GMNC, in association with E2F5, induces expression of *Mci* and *Foxj1* to generate MCC precursors, but does not activate genes for basal body production. Although GMNC interacts with E2F4 far less efficiently than E2F5 in our co-immunoprecipitation assay using overexpressed proteins, this interaction nevertheless seems physiologically relevant as *E2f4* mutant mice exhibit a MCC phenotype in the trachea that is very similar to mice with mutations in GMNC (Danielian et al., 2007; Terré et al., 2016). As the E2F proteins play unique as well as overlapping roles in MCC development in various tissues of the mouse, as well as the zebrafish (Chong et al., 2018; Danielian et al., 2016, 2007), GMNC possibly uses E2F4 or E2F5 in these different contexts to initiate MCC specification. MCI, a protein that is more promiscuous in its ability to interact with the E2F factors, amplifies the expression of *Foxj1* (and genes for other ciliary transcription factors first induced by GMNC) producing a massive upregulation of the motile cilia transcriptional program; more importantly, it activates the genes necessary for the production of multiple basal bodies. This molecular logic helps to clarify why GMNC cannot rescue MCC formation in *Mci* mutant ALI culture, but MCI is sufficient to restore MCC development in *gmnc* mutant zebrafish. Although the C terminus is essential for conferring the differential interaction with E2F proteins, the N-terminal region of GMNC appears to be equally important for its transcriptional ability. The chimeric GM protein not only failed to mimic the transcriptional activation profile of MCI, but also showed an overall impairment in transcriptional

Development (2019) 146, dev172643. doi:10.1242/dev.172643

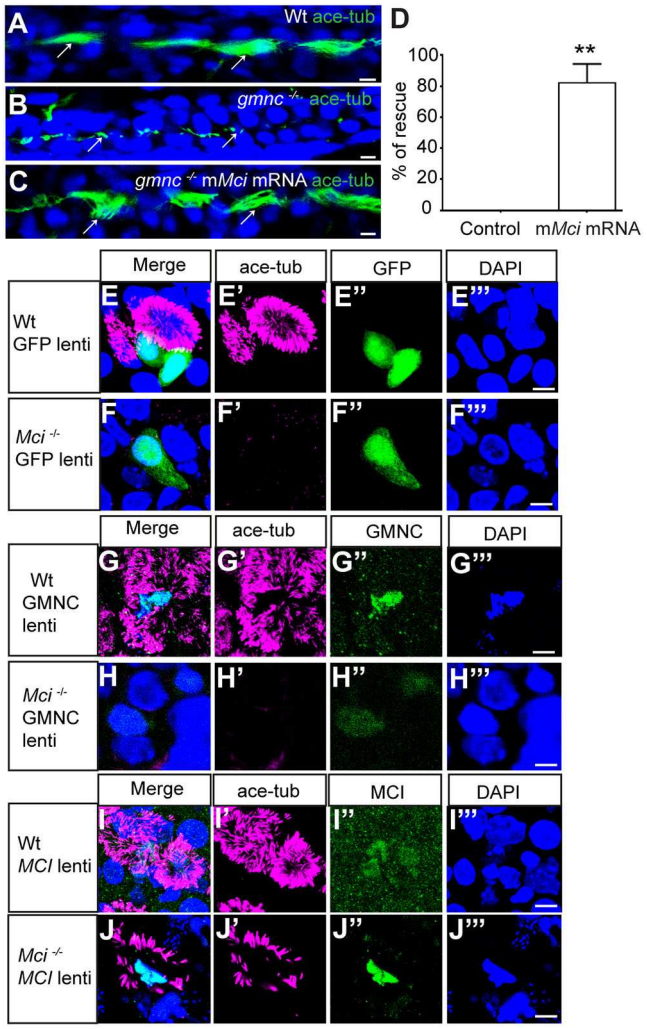

Fig. 8. MCI can substitute for GMNC activity, but not vice versa, in MCC differentiation. (A) Pronephric duct of a 48 h post-fertilization (hpf) wild-type zebrafish embryo showing multiple cilia on MCCs (arrows). (B) Pronephric duct of a 48 hpf *gmnc* mutant zebrafish embryo showing severe lack of MCCs. Monocilia, which are not affected by the loss of Gmnc, are indicated (arrows). (C) Pronephric duct of a 48 hpf *gmnc* mutant embryo showing rescue of MCCs (arrows) on overexpression of mouse *Mci* (m*Mci*) mRNA. (D) Quantification of the rescue of *gmnc* homozygous mutant zebrafish embryos with m*Mci* mRNA. Seventy-two embryos overexpressing mouse MCI were genotyped. Seventeen were *gmnc* homozygotes, of which 14 showed MCC rescue in pronephric ducts (partial to full rescue in one or both ducts). Control represents an uninjected embryo. $^{**}P \leq 0.01$. (E) Lentivirus-mediated overexpression of GFP in wild-type airway cell ALI culture does not affect MCC differentiation (E′-E‴ show individual channels). (F) Overexpression of GFP in *Mci* mutant airway cell ALI culture does not restore MCC differentiation (F′-F‴ show individual channels). (G) Overexpression of GMNC in wild-type airway cell ALI culture induces supernumerary MCC differentiation (G′-G‴ show individual channels). (H) Overexpression of GMNC in *Mci* mutant airway cell ALI culture does not rescue MCC differentiation (H′-H‴ show individual channels). (I) Overexpression of MCI in wild-type airway cell ALI culture induces supernumerary MCC differentiation (I′-I‴ show individual channels). (J) Overexpression of MCI in *Mci* mutant airway cell ALI culture rescues MCC differentiation (J′-J‴ show individual channels). In all preparations, cilia were stained with anti-acetylated tubulin antibodies (green in A-C; magenta in D-I) and nuclei with DAPI (blue). Overexpressed GFP, and GMNC and MCI were detected with anti-GFP and anti-HA antibodies (green in D-I). Lentivirus-mediated overexpression of GFP, MCI and GMNC in ALI cultures represents two independent biological replicates. Scale bars: 5 µm.

activating activity. This implies that either the N-terminal region is important for interacting with other transcriptional co-factors (as the coiled-coil domain resides in this region) or it makes an important contribution to the formation of a functional E2F/DP1 ternary complex. As a corollary of this observation, we propose that the N terminus of MCI could also have a similar role in determining its transcriptional activity. As the precise mechanism by which the MCI/GMNC-E2F-DP1 complex regulates transcription is not understood, and it is also not clear whether other co-factors are involved (particularly in the regulation of the distinct sets of target genes), further biochemical experiments will be necessary to resolve all of these issues.

In conclusion, our study of the *Mci* mutant mouse will be of direct relevance to the role of MCCs in ciliopathies, especially for the pathobiology of RGMC, a relatively new but acute airway disease that remains rather poorly defined. In addition, the sufficiency of GMNC and MCI to generate ectopic MCCs provides a powerful avenue for devising strategies for restoration of functional ciliated epithelia in different MCC-bearing tissues of individuals with ciliopathy by gene therapy. This holds promise not only for rare disorders such as RGMC, but also in acquired and more prevalent airway pathologies such as chronic obstructive pulmonary disorder (COPD), where impairment of ciliary function has also been implicated (Yaghi and Dolovich, 2016).

MATERIALS AND METHODS

Ethics approvals

All mouse and zebrafish experimentation was performed under approval from the Singapore National Advisory Committee on Laboratory Animal Research and conformed to the stipulated ethical guidelines.

Generation of *Mci* knockout mice

Mci mutant mice were generated using CRISPR/Cas9-mediated deletion of a DNA fragment within exon 2 of the *Mci* gene. Two guide RNAs (gRNAs) were designed to target exon 2, and were co-injected with Cas9 mRNA (25 ng/µl) into C57BL/6 one-cell embryos at a concentration of 15 ng/µl each (see Table S1 for sequences of gRNAs and all primers used in this study). A total of 247 embryos were injected, out of which 130 were implanted into nine pseudo-pregnant females. Founder animals were screened by PCR, and mutations were determined first by T7 endonuclease I assay, and then by deep sequencing of PCR products (for selected founders). Out of 13 pups born alive, nine were found to contain mutations at the *Mci* targeted region. Founders containing the desired mutation were bred with the wild-type C57BL/6J animals to produce F1 heterozygotes. The F1 mutants were identified by PCR and confirmed by sequencing.

Zebrafish strains

The AB strain was used as the wild type for all experiments. The *gmnc* mutant strain has been described previously (Zhou et al., 2015).

DNA constructs

Coding sequences for human and mouse DP1, E2F4 and E2F5 were cloned into the pCS2 vector with 6× Myc-tags at the N terminus. Coding sequences for human and mouse GMNC and MCI were cloned into the pXJ40 vector with one HA tag at the N terminus. The human GM chimera was generated using overlapping extension PCR, and cloned into pXJ40 vector with one HA tag at the N terminus.

Co-immunoprecipitation and immunoblot

Desired combinations of plasmids were co-transfected into HEK293T cells, in 10 cm dishes (3 µg per plasmid, per dish) using Lipofectamine 2000 (Thermo Fisher Scientific). After 24 h of incubation, transfected cells were lysed in 800 µl of RIPA buffer (Thermo Fisher Scientific) supplemented with cOmplete, Mini, EDTA-free Protease Inhibitor Cocktail (Roche,

Development (2019) 146, dev172643. doi:10.1242/dev.172643

11836170001). The cell lysates were sonicated briefly and spun down. An aliquot was taken from the clear cell lysate and boiled in 1× SDS loading buffer as input (TCL), and the rest was rotated overnight with 25 µl of Protein A-agarose beads (Roche) and 2 µg of mouse anti-HA antibody (monoclonal, Santa Cruz, SC7392). The beads were washed four times in the immunoprecipitation (IP) buffer and boiled in 50 µl of 1× SDS loading buffer (IP:HA). Both TCL (15 µl, 1%) and IP (15 µl, 30%) were resolved using SDS-PAGE gels, transferred to PVDF membranes, blocked in 2% BSA and probed with relevant primary antibodies [rabbit anti-HA (Santa Cruz, SC805) and rabbit-anti-Myc (Santa Cruz, SC289)] and secondary antibodies [anti-mouse HRP conjugate (Promega, W4028) and anti-rabbit HRP conjugate (Promega, W4018)].

Antibodies

Primary antibodies used were: mouse-anti-HA [Santa Cruz SC7392, 1:2500 for western blot, 1:500 for immunofluorescence (IF)]; rabbit-anti-HA (Santa Cruz SC805, 1:2500 for western blot, 1:500 for IF); mouse-anti-Myc (Santa Cruz SC40, 1:2500 for western blot); rabbit-anti-Myc (Santa Cruz SC289, 1:2500 for western blot); mouse-anti-acetylated-α-tubulin (Sigma-Aldrich, T6793, 1:500 for IF); mouse-anti-α-tubulin (Sigma-Aldrich T6557, 1:500 for IF); mouse-anti-γ-tubulin (Sigma-Aldrich, T6557, 1:500 for IF); rabbit-anti-γ-tubulin (Sigma-Aldrich T5192, 1:500 for IF); rabbit-anti-RFX2 (Sigma-Aldrich, HPA048969, 1:250 for IF), rabbit-anti-RFX3 (Sigma-Aldrich, HPA035689, 1:250 for IF); rabbit-anti-FOXJ1 (Sigma-Aldrich, HPA 005714, 1:250 for IF); mouse anti-FOXJ1 (eBiosciences, 14-9965-80, 1:100 for IF); rabbit-anti-TAP73 (Abcam, ab40658, 1:250 for IF); rabbit-anti-RSPH1(Sigma-Aldrich, HPA017382, 1:250 for IF); rabbit-anti-RSPH9 (Sigma-Aldrich, HPA031703, 1:250 for IF); rabbit-anti-CCDC40 (Sigma-Aldrich, HPA022974, 1:250 for IF); rabbit-anti-pericentrin (Abcam, ab4448, 1:250 for IF); mouse anti-centrin (EMD Millipore, 04-1624, 1:200 for IF), rabbit anti-GFP (Santa Cruz, SC8334, 1:1000 for IF); and rabbit-anti-DEUP1 (kind gift from X. Zhu, Shanghai Institute of Biochemistry and Cell Biology, 1:200 for IF). Secondary antibodies (all used at 1:500 for IF)used were: Alexa 488 goat-anti mouse (Invitrogen A-11029); Alexa 488 goat anti-rabbit (Invitrogen A-11034); Alexa 555 goat anti-rabbit (Invitrogen A-21428); and Alexa 555 goat anti-mouse (Invitrogen A-28180).

Histopathological analysis

To assess hydrocephalus, coronal cryosections of wild-type and *Mci* mutant mouse brains were stained with Hematoxylin and Eosin (H&E) following routine procedures.

Cell and ALI culture

HEK293T and HEK293FT cells were cultured in DMEM with 4500 mg/l glucose and 10% FBS (HyClone, SH30071.03HI). mTEC culture was performed according to a published protocol (Vladar and Brody, 2013). Briefly, mTEC cells were grown on transwells with transparent PET membrane (Life Science, 353095) in mTEC plus+RA medium (DMEM/F12; Life Science, 11330-032), fungizone (Life Technologies, 15290-018, 0.1% v/v), insulin (Sigma-Aldrich, I1882, 10 mg/ml), epidermal growth factor (BD Biosciences, 354001, 25 ng/ml), transferrin (Sigma T1147, 5 mg/ml), cholera toxin (Sigma-Aldrich C8052, 0.1 mg/ml), fetal bovine serum (Life Technologies 26140-079, 5% v/v), ROCK inhibitor (ATCCY27632 ,10 µM), retinoic acid (Sigma-Aldrich R2625, 50 nM) and penicillin-streptomycin (Life Technologies, 15140-148, 100 U penicillin, 100 mg streptomycin per ml). When cells on the apical side of the transwell chambers reached 100% confluence, ALI was established by aspirating the culture medium from the transwell chambers, and addition of differentiation medium (mTEC Plus medium without fetal bovine serum and ROCK inhibitor) to the basal chamber on 24-well plates. The mTEC cells were maintained on transwells by changing the differentiation medium in the basal chamber every 2 days.

Immunofluorescence

For IF analysis, mTEC cells grown on transwells were fixed in 4% paraformaldehyde (PFA) at room temperature for 10 min, permeabilized with PBTX (PBS, 0.5% Triton X-100) for 2 h and washed in phosphate-buffered saline (PBS). Cells were then blocked with 2% bovine serum albumin in PBS for 1 h, followed by 1 h with primary antibody at room temperature. After three washes in PBS, cells were incubated with secondary antibodies and DAPI for 1 h. After briefly washing with PBS, the cells were mounted on glass slides with fluorescence-mounting medium and imaged using an Olympus FluoView upright laser scanning confocal microscope. Cryosections of mouse tissues were prepared by the histopathology unit and the slides stored at −80°C. On the day of staining, slides were thawed and dried before drawing borders around the sections with a PAP pen (Abcam, ab2601). The slides were then fixed with 4% PFA for 15 min at room temperature in Coplin jars (all subsequent steps were performed in Coplin jars unless stated otherwise), rinsed twice with ice-cold PBS followed by permeabilization with 0.2% Triton (in PBS) for 15 min. Next, slides were washed 3 times, 5 min each in PBS and blocked with 2% BSA in PBS for 2 h at room temperature. The slides were then transferred to a humidified box. Primary antibodies in PBS (with 0.1% Tween20 and 1% BSA) were pipetted onto the sections and incubated overnight at 4°C. The following day, slides were washed with PBS on a shaker, six times for 10 min each at room temperature. Secondary antibodies in PBS (with 0.1% Tween20 and 1% BSA) were then added, and the slides incubated in the humidified box for 5 h at room temperature. Finally, the slides were washed six times (10 min each) with PBS at room temperature, dried and mounted using Vectashield.

RT-qPCR

cDNA preparations were generated using the SuperScript III First-Strand Synthesis System (Invitrogen 18080051). Gene-specific primers for qPCR were designed using the Primer3 software (Primer3 v.0.4.0) and are listed in Table S1. qPCR was performed using the EXPRESS SYBR GreenER Super Mix (Invitrogen, A10315) on an Applied BioSystems 7900HT Fast Real-Time PCR System using SDS2.4 software. Technical triplicate reactions were performed for each sample. Using Microsoft Excel, gene expression fold differences were calculated from the Ct values after normalizing against the internal control *Gapdh*/*GAPDH*.

Microinjection of zebrafish eggs and processing for IF analysis

mRNA encoding mouse MCI (300 ng/µl, 0.75 nl per egg) was injected into one-cell stage eggs derived from in-cross of *gmnc* heterozygous fish. At 48 h post fertilization (hpf), the injected embryos were fixed with Dent's fixative (80% methanol, 20% DMSO) for 3 h at room temperature and then subjected to IF staining using routine protocol.

Lentivirus generation and infection

Gene expression lentiviruses were generated using ViraPower Lentiviral Expression Systems Version C (Invitrogen, 25-0501). Briefly, coding sequences of different genes were cloned into PLVX vector, followed by transfection into HEK293FT cells together with the Lentiviral Packaging Mix (Invitrogen, K4975-00). Viruses were harvested by collecting the cell culture medium 3 days after transfection. Viral titration was performed by infecting 293FT cells with the control GFP lentivirus, which was generated together with gene-specific expression lentiviruses (*GMNC* and *MCI*), and then determined by the percentage of GFP-positive cells 3 days after infection. For confluent mTEC cells viral infection, the cells were treated with 12 mM EGTA (Sigma-Aldrich, E3889) in 10 mM HEPES (Sigma-Aldrich, H3375-25G) at pH 7.4 for 25 min at 37°C. After washing the EGTA-treated cells with PBS, a mix of specific amounts of lentivirus and Polybrene (Sigma-Aldrich, H9268, 5 µg/ml final concentration) was added into the culture medium. mTEC cells with the viruses were then centrifuged at 1500 ***g*** for 80 min at 32°C, and grown at 37°C in a cell culture incubator.

Electron microscopy of mouse trachea

For SEM analysis, mouse tracheae were fixed immediately after dissection by immersion in 4% formaldehyde and 2% glutaraldehyde (EM grade, Electron Microscopy Sciences) in 0.1 M sodium cacodylate buffer (pH 7.4) for 12 h. After washing, samples were cut across the length into ∼2 mm pieces, and subsequently cut longitudinally to expose the interior surface. Trimmed samples were post-fixed with 1% osmium tetroxide in distilled water for 2 h, washed with distilled water and dehydrated in an ethanol

series. Dehydrated samples were dried using critical point drying (Leica EM CPD030), mounted onto aluminium stubs with trachea lumen facing up and sputter coated with 4 nm layer of platinum (Leica EM SCD050). SEM analysis was performed using a JSM 6701F SEM (JEOL) microscope operating at 2.5 kV. Images were collected from random areas of the wild-type and mutant samples. For TEM analysis, dissected tracheae were fixed in 4% paraformaldehyde, 2.5% glutaraldehyde and 0.2% picric acid in 0.1 M sodium cacodylate buffer. Samples were washed in sodium cacodylate buffer and post fixed with 1% osmium tetroxide. Samples were washed again in sodium cacodylate buffer before dehydration through a graded series of ethanol. After dehydration, samples were infiltrated and embedded with Spurr resin (Electron Microscopy Sciences 14300) before polymerization at 60°C. Ultra-thin sections were obtained by cutting sample blocks on an ultramicrotome (Leica ultracut UCT), stained with 4% uranyl acetate and 2% lead citrate before viewing the sections using a TEM (Jeol 1010) microscope.

Statistical analysis

The statistical analysis, including standard error of the mean (s.e.m.), standard deviation (s.d.) and unpaired *t*-test, was performed using the software GraphPad Prism 7.04.

Acknowledgements

We thank the Animal Gene Editing Laboratory, Biological Resource Centre, Agency for Science, Technology and Research for generating the *Mci* mutant mice; the Advanced Molecular Pathology Laboratory for histological services; the Institute of Medical Biology – Institute of Molecular and Cell Biology Joint Electron Microscopy Suite for electron microscopy analysis; the Institute of Molecular and Cell Biology Zebrafish Facility for maintenance of zebrafish strains; the DNA Sequencing Facility for the sequencing service; V. Tergaonkar for assistance in obtaining appropriate clearance from the Institutional Animal Care and Use Committee (IACUC) for experiments with the *Mci* mutant mice; X. Zhu for DEUP1 antibodies; and A. Guha, T. Stracker and members of our laboratory for discussion and insightful comments on the manuscript.

Competing interests

The authors declare no competing or financial interests.

Author contributions

Conceptualization: H.L., S.R.; Methodology: H.L., C.D.B., S.R.; Validation: H.L., P.A., F.Z., Y.Z., Y.L.C., C.D.B., S.R.; Formal analysis: H.L., P.A., F.Z., Y.Z., Y.L.C.; Investigation: H.L., P.A., F.Z., Y.Z., Y.L.C.; Resources: H.L.; Data curation: S.R.; Writing - original draft: S.R.; Writing - review & editing: H.L., C.D.B., S.R.; Supervision: C.D.B., S.R.; Project administration: S.R.; Funding acquisition: S.R.

Funding

P.A. was supported by a University of Sheffield–Agency for Science, Technology and Research (A*STAR), Singapore doctoral studentship. This work was supported by funds from the Agency for Science, Technology and Research to S.R.

Supplementary information

Supplementary information available online at
http://dev.biologists.org/content/146/6/dev172643.supplemental

References

Al Jord, A., Lemaitre, A.-I., Delgehyr, N., Faucourt, M., Spassky, N. and Meunier, A. (2014). Centriole amplification by mother and daughter centrioles differs in multiciliated cells. *Nature* **516**, 104-107.

Arbi, M., Pefani, D.-E., Kyrousi, C., Lalioti, M.-E., Kalogeropoulou, A., Papanastasiou, A. D., Taraviras, S. and Lygerou, Z. (2016). GemC1 controls multiciliogenesis in the airway epithelium. *EMBO Rep.* **17**, 400-413.

Becker-Heck, A., Zohn, I. E., Okabe, N., Pollock, A., Lenhart, K. B., Sullivan-Brown, J., Mcsheene, J., Loges, N. T., Olbrich, H., Haeffner, K. et al. (2011). The coiled-coil domain containing protein CCDC40 is essential for motile cilia function and left-right axis formation. *Nat. Genet.* **43**, 79-84.

Boon, M., Wallmeier, J., Ma, L., Loges, N. T., Jaspers, M., Olbrich, H., Dougherty, G. W., Raidt, J., Werner, C., Amirav, I. et al. (2014). MCIDAS mutations result in a mucociliary clearance disorder with reduced generation of multiple motile cilia. *Nat. Commun.* **5**, 4418.

Brooks, E. R. and Wallingford, J. B. (2014). Multiciliated cells. *Curr. Biol.* **24**, R973-R982.

Bustamante-Marin, X. M. and Ostrowski, L. E. (2017). Cilia and mucociliary clearance. *Cold Spring Harb. Perspect. Biol.* **9**, a028241.

Choksi, S. P., Babu, D., Lau, D., Yu, X. and Roy, S. (2014a). Systematic discovery of novel ciliary genes through functional genomics in the zebrafish. *Development* **141**, 3410-3419.

Choksi, S. P., Lauter, G., Swoboda, P. and Roy, S. (2014b). Switching on cilia: transcriptional networks regulating ciliogenesis. *Development* **141**, 1427-1441.

Chong, Y. L., Zhang, Y., Zhou, F. and Roy, S. (2018). Distinct requirements of E2f4 versus E2f5 activity for multiciliated cell development in the zebrafish embryo. *Dev. Biol.* **443**, 165-172.

Danielian, P. S., Bender Kim, C. F., Caron, A. M., Vasile, E., Bronson, R. T. and Lees, J. A. (2007). E2f4 is required for normal development of the airway epithelium. *Dev. Biol.* **305**, 564-576.

Danielian, P. S., Hess, R. A. and Lees, J. A. (2016). E2f4 and E2f5 are essential for the development of the male reproductive system. *Cell Cycle* **15**, 250-260.

Frommer, A., Hjeij, R., Loges, N. T., Edelbusch, C., Jahnke, C., Raidt, J., Werner, C., Wallmeier, J., Grosse-Onnebrink, J., Olbrich, H. et al. (2015). Immunofluorescence analysis and diagnosis of primary ciliary dyskinesia with radial spoke defects. *Am. J. Respir. Cell Mol. Biol.* **53**, 563-573.

Funk, M. C., Bera, A. N., Menchen, T., Kuales, G., Thriene, K., Lienkamp, S. S., Dengjel, J., Omran, H., Frank, M. and Arnold, S. J. (2015). Cyclin O (Ccno) functions during deuterosome-mediated centriole amplification of multiciliated cells. *EMBO J.* **34**, 1078-1089.

Jackson, P. K. and Attardi, L. D. (2016). p73 and FoxJ1: programming multiciliated epithelia. *Trends Cell Biol.* **26**, 239-240.

Klos Dehring, D. A., Vladar, E. K., Werner, M. E., Mitchell, J. W., Hwang, P. and Mitchell, B. J. (2013). Deuterosome mediated centriole biogenesis. *Dev. Cell* **27**, 103-112.

Knowles, M. R., Zariwala, M. and Leigh, M. (2016). Primary ciliary dyskinesia. *Clin. Chest Med.* **37**, 449-461.

Kyrousi, C., Arbi, M., Pilz, G.-A., Pefani, D.-E., Lalioti, M.-E., Ninkovic, J., Gotz, M., Lygerou, Z. and Taraviras, S. (2015). Mcidas and GemC1 are key regulators for the generation of multiciliated ependymal cells in the adult neurogenic niche. *Development* **142**, 3661-3674.

Ma, L., Quigley, I., Omran, H. and Kintner, C. (2014). Multicilin drives centriole biogenesis via E2f proteins. *Genes Dev.* **28**, 1461-1471.

Mercey, O., Al Jord, A., Rostaing, P., Mahuzier, A., Fortoul, A., Boudjema, A.-R., Faucourt, M., Spassky, N. and Meunier, A. (2018). Dynamics of centriole amplification in centrosome-depleted brain multiciliated progenitors. *bioRxiv*, 503730.

Nanjundappa, R., Kong, D., Shim, K., Stearns, T., Brody, S., Loncarek, J. and Mahjoub, M. (2018). Regulation of cilia abundance in multiciliated cells. *bioRxiv*, 478297.

Revinski, D. R., Zaragosi, L.-E., Boutin, C., Ruiz-Garcia, S., Deprez, M., Thomé, V., Rosnet, O., Gay, A.-S., Mercey, O., Paquet, A. et al. (2018). CDC20B is required for deuterosome-mediated centriole production in multiciliated cells. *Nat. Commun.* **9**, 4668.

Spassky, N. and Meunier, A. (2017). The development and functions of multiciliated epithelia. *Nat. Rev. Mol. Cell Biol.* **18**, 423-436.

Stubbs, J. L., Oishi, I., Izpisúa Belmonte, J. C. and Kintner, C. (2008). The forkhead protein Foxj1 specifies node-like cilia in Xenopus and zebrafish embryos. *Nat. Genet.* **40**, 1454-1460.

Stubbs, J. L., Vladar, E. K., Axelrod, J. D. and Kintner, C. (2012). Multicilin promotes centriole assembly and ciliogenesis during multiciliate cell differentiation. *Nat. Cell Biol.* **14**, 140-147.

Terré, B., Piergiovanni, G., Segura-Bayona, S., Gil-Gómez, G., Youssef, S. A., Attolini, C. S.-O., Wilsch-Bräuninger, M., Jung, C., Rojas, A. M., Marjanović, M. et al. (2016). GEMC1 is a critical regulator of multiciliated cell differentiation. *EMBO J.* **35**, 942-960.

Vladar, E. K. and Brody, S. L. (2013). Analysis of ciliogenesis in primary culture mouse tracheal epithelial cells. *Methods Enzymol.* **525**, 285-309.

Yaghi, A. and Dolovich, M. B. (2016). Airway epithelial cell cilia and obstructive lung disease. *Cells* **5**, pii: E40.

Yu, X., Ng, C. P., Habacher, H. and Roy, S. (2008). Foxj1 transcription factors are master regulators of the motile ciliogenic program. *Nat. Genet.* **40**, 1445-1453.

Zhao, H., Zhu, L., Zhu, Y., Cao, J., Li, S., Huang, Q., Xu, T., Huang, X., Yan, X. and Zhu, X. (2013). The Cep63 paralogue Deup1 enables massive de novo centriole biogenesis for vertebrate multiciliogenesis. *Nat. Cell Biol.* **15**, 1434-1444.

Zhao, H., Chen, Q., Huang, Q., Yan, X. and Zhu, X. (2018). Mother centrioles are dispensable for deuterosome formation and function during basal body amplification. *bioRxiv*.

Zhou, F. and Roy, S. (2015). SnapShot: motile cilia. *Cell* **162**, 224-224.e1.

Zhou, F., Narasimhan, V., Shboul, M., Chong, Y. L., Reversade, B. and Roy, S. (2015). Gmnc is a master regulator of the multiciliated cell differentiation program. *Curr. Biol.* **25**, 3267-3273.

SUPPLEMENTAL INFORMATION

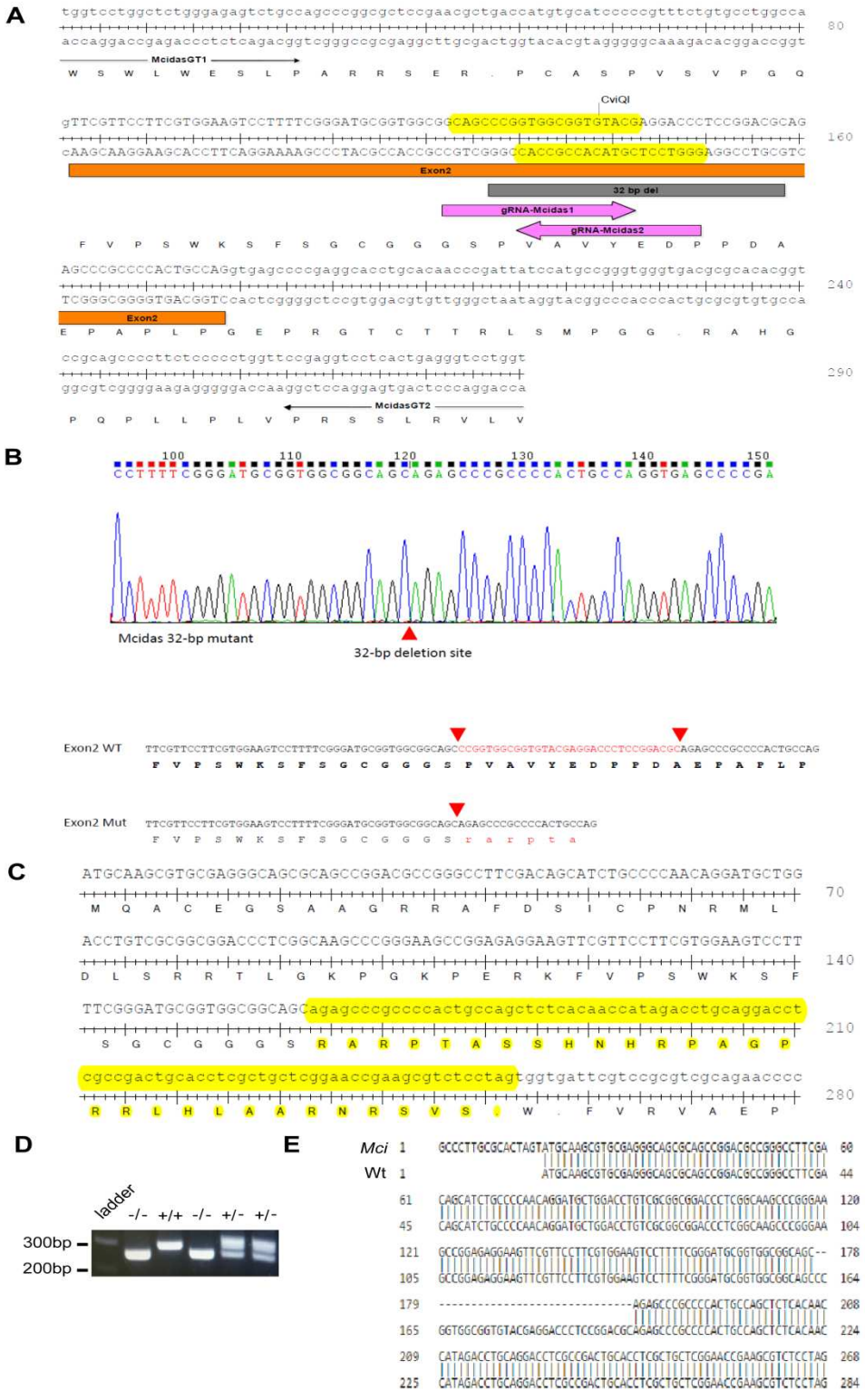

Development • Supplementary information

Fig. S1. Generation of a deletion allele at the mouse *Mci* locus. (A) Partial genomic sequence of the mouse *Mci* gene, showing the gRNAs (pink arrows) and their target sites on the forward and reverse strands (highlighted in yellow) used to induce a 32 bp deletion within exon 2. Binding sites for genotyping primers (McidasGT1 and McidasGT2) are also indicated. (B) Electropherogram showing 32 bp deletion in *Mci* exon 2. Also shown below is the conceptual translation of the wild-type and mutant *Mci* coding sequence around the deletion site. (C) Conceptual translation of the predicted mutant *Mci* ORF shows a highly truncated MCI protein, retaining only 54 native amino acids at the N-terminus. Sequences highlighted in yellow indicate disruption of the reading frame before the premature STOP codon. (D) Gel image of DNA fragments amplified in wild-type, heterozygote and homozygous *Mci* mutants using primers flanking the 32 bp deletion. Size of the wild-type band is 290 bp and the mutant band is 258 bp. (E) Sequence analysis of *Mci* cDNA obtained from tracheal tissue of the homozygous mutants confirms a deletion of 32 bp.

Development • Supplementary information

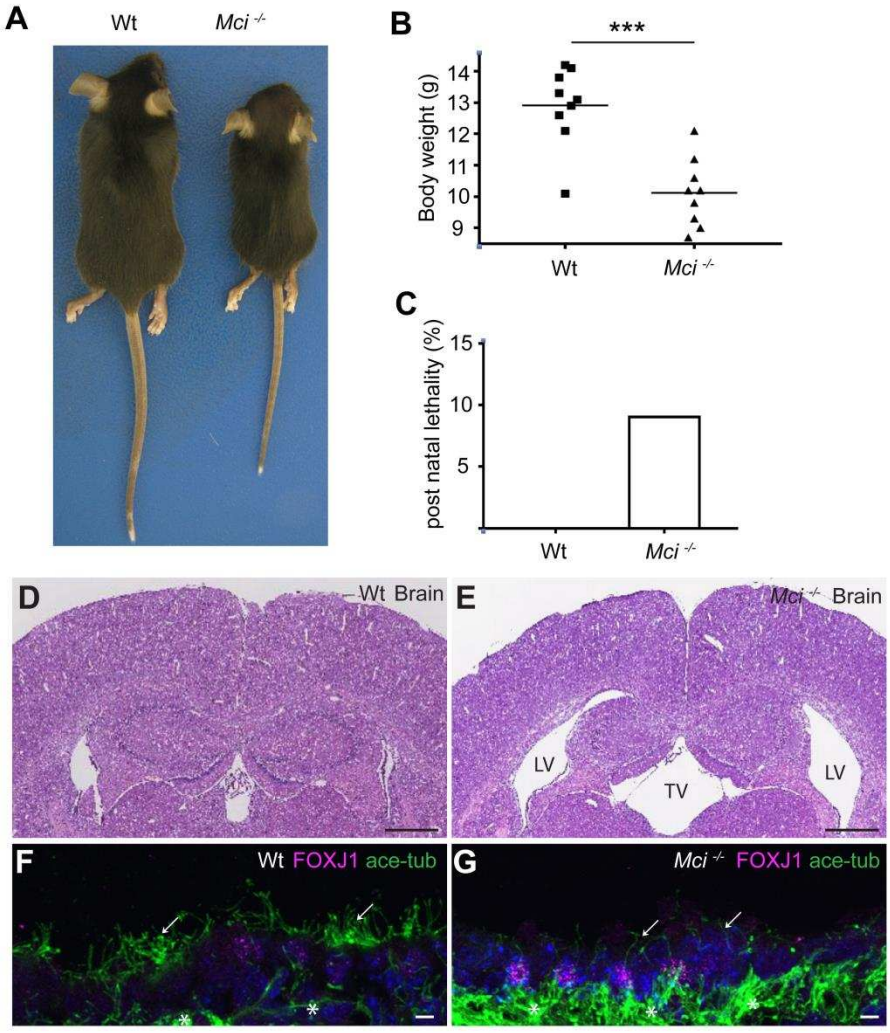

Fig. S2. Gross phenotypes of *Mci* knockout mice. (A) *Mci* knockout mice are smaller in size compared to the wild-type. (B) The body weight comparison between wild-type and *Mci* mutant mice at post-natal day (P) 28. $n = 9$ for each genotype. (C) Percentage of lethality of wild type and *Mci* knockout mice at P28. $n = 22$ for each genotype. (D) Wild-type mouse brain coronal section stained with H&E. (E) *Mci* mutant mouse brain coronal section stained with H&E. Note hydrocephalus with dilation of the lateral

Development • Supplementary information

ventricles (LV) and the third ventricle (TV). Scale bar = 1mm. (F) Nuclear localized FOXJ1 expression in MCCs of wild-type brain ependyma. Multicilia are indicated by arrows and the cytoskeletal microtubule network by asterisks. (G) Nuclear localized FOXJ1 expression in monociliated cells of *Mci* mutant brain ependyma. Monocilia are indicated by arrows and the cytoskeletal microtubule network by asterisks. Scale bars, 5 μm.

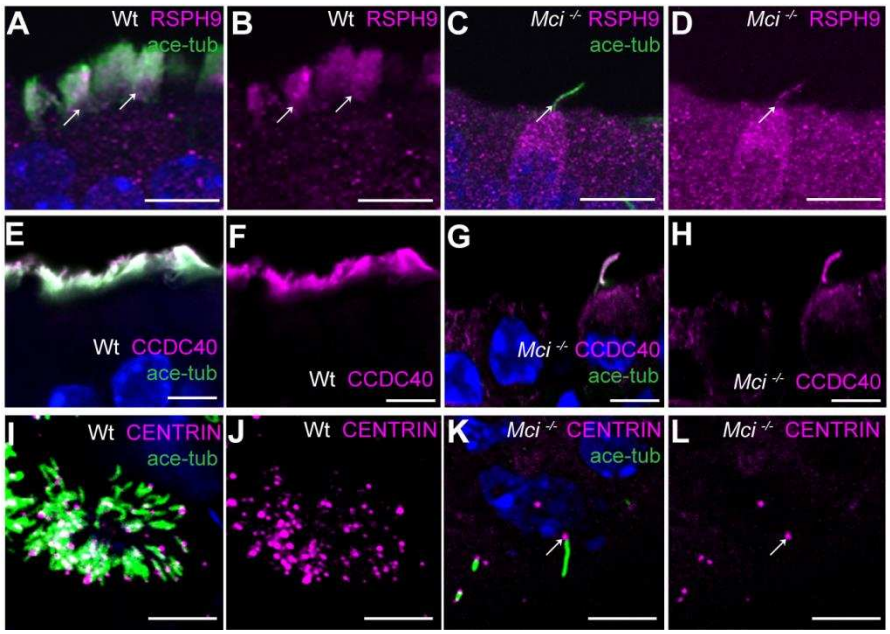

Fig. S3. *Mci* mutant MCCs precursors differentiate a single cilium that localizes motile cilia-specific proteins but are unable to make multiple basal bodies. (A) RSPH9 co-localization with acetylated tubulin to MCC cilia of wild-type trachea (arrows). (B) RSPH9 localization to MCC cilia of wild-type trachea (arrows; display of only RSPH9 staining from panel A). (C) RSPH9 co-localization with acetylated tubulin

Development • Supplementary information

to single cilium of *Mci* mutant trachea (arrow). (D) RSPH9 localization to single cilium of *Mci* mutant trachea (arrow; display of only RSPH9 staining from panel C). (E) CCDC40 co-localization with acetylated tubulin to MCC cilia of wild-type trachea (arrows). (F) CCDC40 localization to MCC cilia of wild-type trachea (arrows; display of only CCDC40 staining from panel A). (G) CCDC40 co-localization with acetylated tubulin to single cilium of *Mci* mutant trachea (arrow). (H) CCDC40 localization to single cilium of *Mci* mutant trachea (arrow; display of only CCDC40 staining from panel C). (I) Wild-type MCC differentiated in ALI culture with multiple basal bodies (stained with anti-CENTRIN antibodies) and multiple cilia. (J) Display of only CENTRIN staining from panel E. (K) *Mci* mutant cells differentiated in ALI culture with single basal body (expressing CENTRIN, arrow) and single cilium. (L) Display of only CENTRIN staining from panel G showing single basal body (arrow). In all preparations, cilia were stained with anti-acetylated tubulin antibodies (green) and nuclei with DAPI (blue). Scale bars A-D = 10 μm; E-L = 5 μm.

Development • Supplementary information

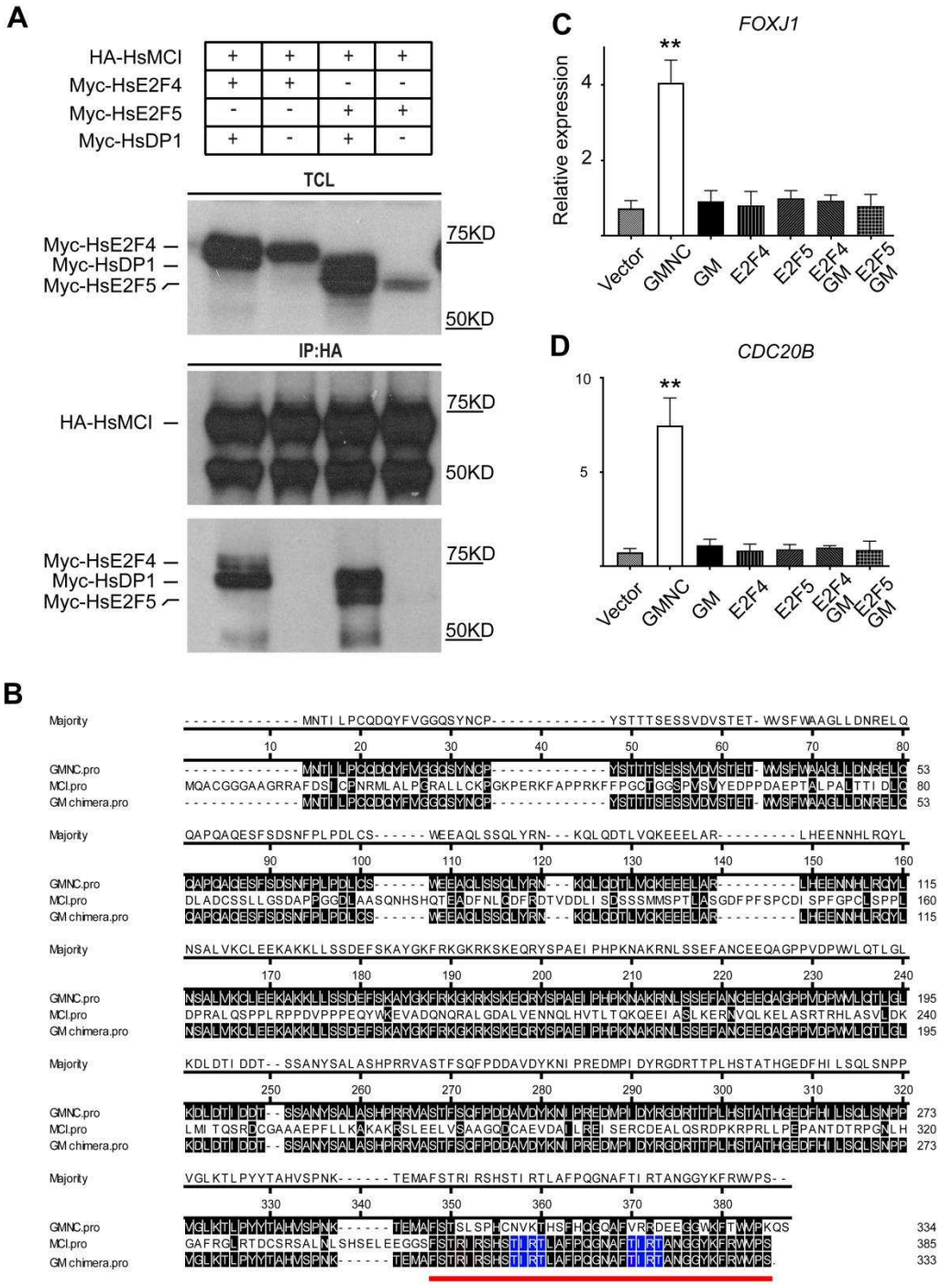

Fig. S4. Interaction of MCI with E2F factors and transcriptional activity of the GMNC-MCI chimeric protein in HEK293T cells. (A) Co-immunoprecipitation data

Development • Supplementary information

showing interaction of MCI with E2F4 as well as E2F5. Human proteins were used for this experiment. (B) Amino acid sequence alignment of human GMNC, MCI and GM proteins. The C-terminal TIRT domain from MCI used to generate GM is underlined in red, and the TIRT resides in MCI and GM proteins are highlighted in blue. (C) Unlike wild-type GMNC, the GM chimeric protein is unable to induce *FOXJ1* expression by itself or together with the E2F factors. (D) The GM protein is not more efficient in inducing *CDC20B* expression than wild-type GMNC either by itself or with the E2F factors. For C and D, relative expression levels have been plotted along the *y*-axis, and overexpression conditions indicated along the *x*-axis. Error bars: SEM. Immunoblot and qPCR data are representative of 2 independent biological replicates. p: ** ≤ 0.01.

Development • Supplementary information

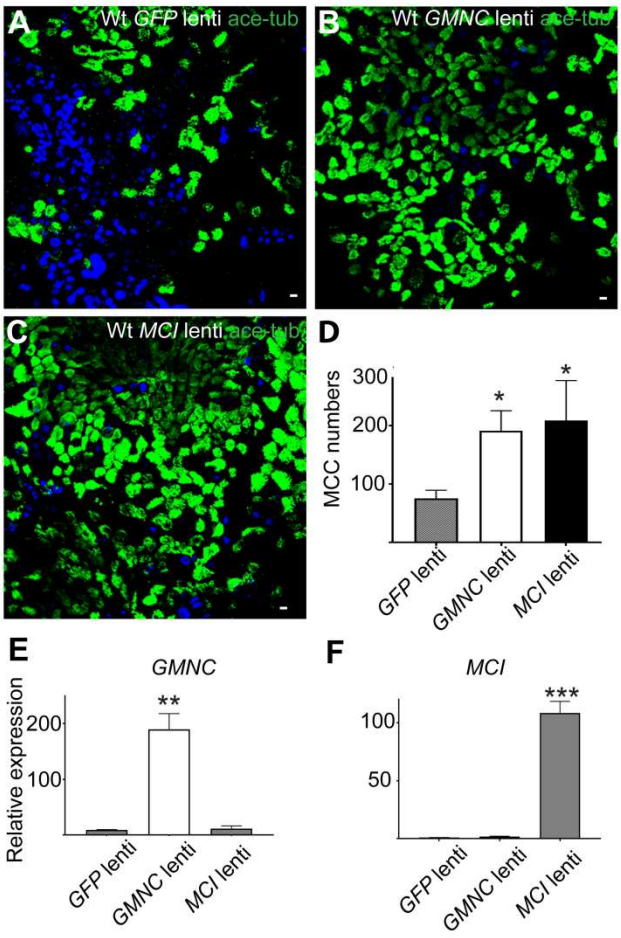

Fig. S5. Overexpression of GMNC and MCI in wild-type airway cell ALI culture induces supernumerary MCCs. (A) Lentivirus mediated overexpression of GFP in wild-type airway cell ALI culture does not affect numbers of differentiating MCCs. (B) Overexpression of GMNC in wild-type airway cell ALI culture induces supernumerary MCCs. (C) Overexpression of MCI in wild-type airway cell ALI culture induces supernumerary MCCs. Scale bars, 5 μm. (D) Quantification of MCC numbers per field of view upon overexpression of GFP, GMNC and MCI in wild-type airway cell ALI

Development • Supplementary information

cultures. (E,F) RT-qPCR analysis of GMNC and MCI expression levels on overexpression of GMNC and MCI in *Mci* mutant airway cells cultured under ALI conditions. Relative expression levels have been plotted along the *y*-axis, and overexpression conditions indicated along the *x*-axis. Lentivirus-mediated overexpression of GFP, MCI and GMNC in ALI cultures represent 2 independent biological replicates; qPCR analysis represents 2 independent technical replicates. Error bars: SEM. p: * ≤ 0.05, ** ≤ 0.01, *** ≤0.001.

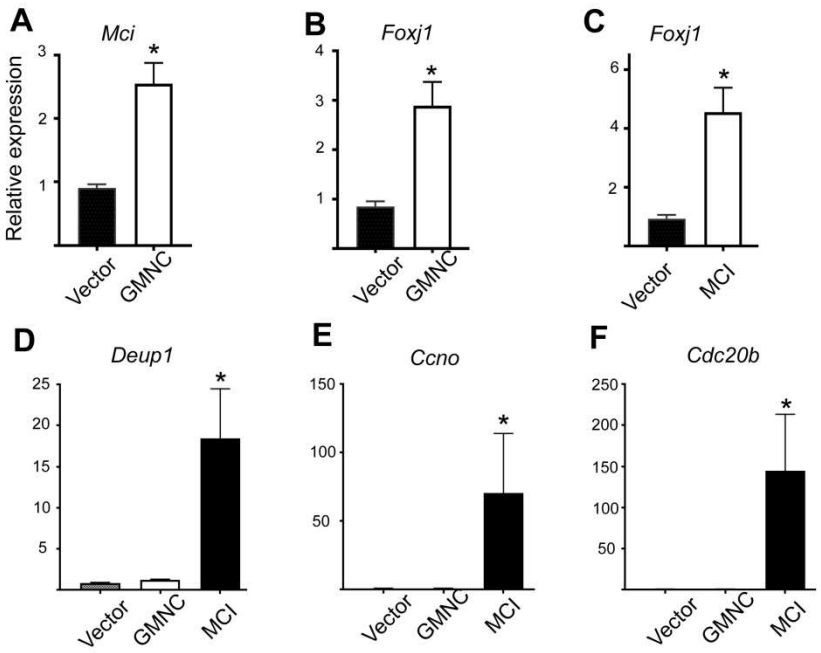

Fig. S6. RT-qPCR analysis of ciliary transcription factor and DD pathway genes expression levels on overexpression of MCI and GMNC in *Mci* mutant airway cells

Development • Supplementary information

cultured under ALI conditions. (A-F) Relative expression levels have been plotted along the *y*-axis, and overexpression conditions indicated along the *x*-axis. Error bars represent SEM. Analysis was done on 3 independent biological replicates. p: * ≤ 0.05.

Table S1. Primer seqences

Name of gRNA/primer	**Sequence (5′-3′)**	**Remarks**
gRNA-Mcidas1	CAGCCCGGTGGCGGTGTACGGTTTTAGAGCTAGAAATAGCAAGTTAAAATAAGGCTAGTCCGTTATCAACTTGAAAAAGTGGCACCGAGTCGGTGCTTT	gRNA sequences
gRNA-Mcidas2	GGGTCCTCGTACACCGCCACGTTTTAGAGCTAGAAATAGCAAGTTAAAATAAGGCTAGTCCGTTATCAACTTGAAAAAGTGGCACCGAGTCGGTGCTTT	
McidasGT1(forward)	TGGTCCTGGCTCTGGGAGAGTCTGCC	Primers for genotyping of *Mci* mutant mice
McidasGT2(reverse)	ACCAGGACCCTCAGTGAGGACCTCGG	
Mci-L	CGGAGCAGTACTGGAAGGAG	qPCR primers for mouse genes
Mci-R	TTCGTTGTTGCCTTGATCTG	
Gmnc-L	TCTGGAAGAGAAGGCCAAGA	
Gmnc-R	CCCAGGTTGTTCCTCACAGT	
Foxj1-L	GAGCTGGAACCACTCAAAGG	
Foxj1-R	GGTAGCAGGGCAGTTGATGT	
Rfx2-L	TGTGAGCCGATCCTACAGTG	
Rfx2-R	ACCTTGGTCTGGATGACCTG	
Rfx3-L	CAGACAGTTCAGCAGGTCCA	
Rfx3-R	CTGGGCAGAACTTCCTTGAG	
Deup1-L	AGATGCGGGCTTTAGAGACA	
Deup1-R	CGGTGAATTTGGTTTTGCTT	
Ccno-L	GCTGAGCCTAACGGATTACG	
Ccno-R	TGATGGACACTAGCGTCTGC	

Development • Supplementary information

Cdc20b-L	GAAGGAAAATCTTGCCACCA	
Ccdc20b-R	TTGGCATGTGGAATGGTAGA	
Ccdc78-L	ACCAGGTGCCACCATTAGAG	
Ccdc78-R	AAGCCAGTTGCTGACCAGTT	
Gapdh-L	AACTTTGGCATTGTGGAAGG	
Gapdh-R	ACACATTGGGGGTAGGAACA	
Cep63-L	TCTGTGAGTGCAACATGCAA	
Cep63-R	GAGGAACACTTGGCAGAAGC	
Plk4-L	AAACCAAAAAGGCTGTGGTG	
Plk4-R	GGAGGTCTGTCAGCAAGAGG	
Cep152-L	GCTGTGGACACTGCTTTCAA	
Cep152-R	CACCCTGCTGTTCTCCTCTC	
Sas6-L	CCTGCAGCTTACAAACCAGG	
Sas6-R	CTGGCTAATCCGCGTAAAG	
MCI-L	GCCTGAGCAATACTGGAAGG	qPCR primers for human genes
MCI-R	AGTTCCTTCAGCTGCACGTT	
GMNC-L	CCCAAAAATGCCAAAAGAAA	
GMNC-R	AATGTGCTGGCGACTCTTCT	
FOXJ1-L	CACGTGAAGCCTCCCTACTC	
FOXJ1-R	GGATTGAATTCTGCCAGGTG	
DEUP1-L	CACAAAGAAAGCTGCCCTTC	
DEUP1-R	TCGGAGCCTTTCATTCTCAT	
CCNO-L	TCTACAGACCTTCCGCGACT	
CCNO-R	TCCAGAGTGTTCACCGTCAG	
CDC20B-L	GAAGACACCGCCTGAGAAAG	
CDC20B-R	CACAGAGCTGCATTTTTCCA	
GAPDH-L	GAGTCAACGGATTTGGTCGT	
GAPDH-R	TTGATTTTGGAGGGATCTCG	
GM-N-N	AGTCAGTCAAGCTTATGAAC ACCATTCTGCCT	Primers to generate GMNC N-terminus and MCI C-terminus chimera
GM-C-N	GGATGCGGGTGCTGAATGCCAT CTCTGTCTTG	
GM-N-C	CAAGACAGAGATGGCATTCAGC ACCCGCATCC	
GM-C-C	AGTCAGTCGCGGCCGCACTGGGGA CCCAGCGGAAC	
GMNC-HA-XhoI-pLvx	GATCGATCCTCGAGGCCACCATGT ACCCATACGACGTGCCAGACTACG	Primers to clone HA-

Development • Supplementary information

	CAATGAACACCATTCTGCC	tagged GMNC into PLVX vector
GMNC-C-XbaI-pLvx	GATCGATCTCTAGACTAAGACTGC TTAGGGAC	
MCI-HA-XhoI-pLvx	GATCGATCCTCGAGGCCACCATGT ACCCATACGACGTGCCAGACTACG CAATGCAGGCGTGCGGGGG	Primers to clone HA-tagged MCI into PLVX vector
MCI-C-XbaI-pLvx	GATCGATCTCTAGATCAACTGGG GACCCAGCG	

Development • Supplementary information